AECU-4686

REPORT No. ER-3896

THE SNAP II POWER CONVERSION SYSTEM
TOPICAL REPORT No. 4 TURBINE DESIGN & TESTING

MASTER

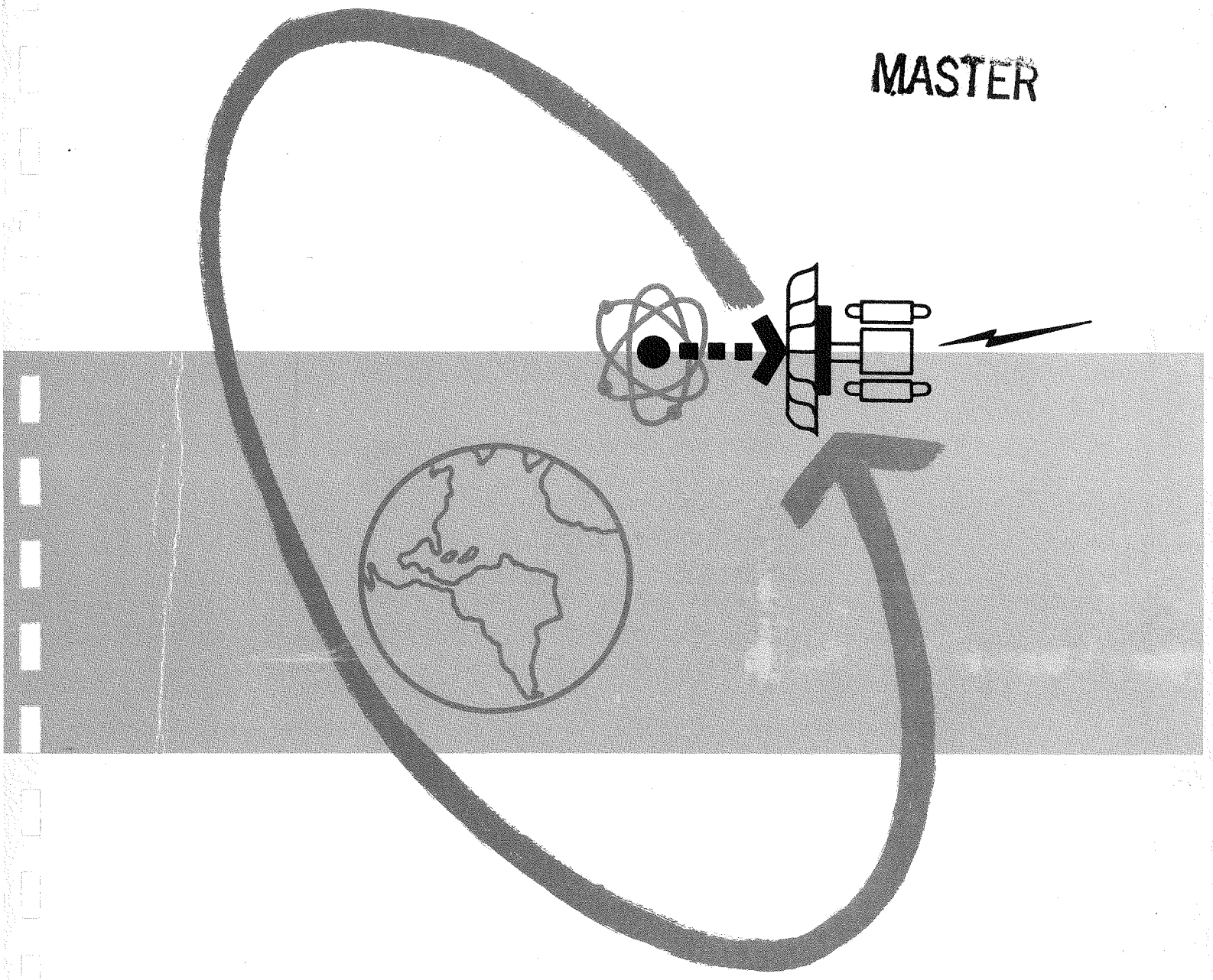

STAFF RESEARCH AND DEVELOPMENT

THOMPSON PRODUCTS DIVISIONS

Thompson Ramo Wooldridge Inc.

CLEVELAND, OHIO

DISCLAIMER

PROJECT

562-137252-88

REPORT NO. ER-3896

THE SNAP II POWER CONVERSION SYSTEM TOPICAL REPORT NO. 4 TURBINE DESIGN AND TESTING

PREPARED BY:	CHECKED BY:	APPROVED BY:
Earnest N. Poulos	George Y. Ono	Walter R. Chapman
Earnest N. Poulos Research Engineer	George Y. Ono Head, Mechanical Section	W.R. Chapman Manager, Engineering
Edward R. Furman	Donald L. Southam	J.E. Taylor
Edward R. Furman Design Engineer	Donald L. Southam Project Manager	J.E. Taylor Manager, New Devices Laboratories

DATE

January 18, 1960

DEPARTMENT

Engineering
New Devices Lab.

Thompson Ramo Wooldridge Inc.

CLEVELAND, OHIO, U. S. A.

LEGAL NOTICE

This report was prepared as an account of Government sponsored work. Neither the United States, nor the Commission nor any person acting on behalf of the Commission:

A. Makes any warranty or representation, expressed or implied, with respect to the accuracy, completeness, or usefulness of the information contained in this report, or that the use of any information, apparatus, method, or process disclosed in this report may not infringe upon privately owned rights; or

B. Assumes any liabilities with respect to the use of, or for damages resulting from the use of information, apparatus, method, or process disclosed in this report.

As used in the above, "person acting on behalf of the Commission" includes any employee or contractor of the Commission to the extent that such employee or contractor prepares, handles or distributes, or provides access to, any information pursuant to his employment or contract with the Commission.

ABSTRACT

SNAP II is the designation for a 3 KW nuclear auxiliary power unit to be used in a satellite vehicle. The SNAP II system consists of a reactor heat source, a mercury Rankine engine, and an alternator. A two stage, full admission, axial flow turbine was chosen for this APU application. Design details and test results are presented in this report. This work was performed under a subcontract to Atomics International as part of the Atomic Energy Commission Contract AT(11-1)-GEN-8.

LIST OF FIGURES

LIST OF TABLES

SUMMARY

The SNAP II system is a 3 KW nuclear auxiliary power unit intended to be used in a satellite vehicle. The SNAP II powerplant utilizes a mercury vapor Rankine cycle with a reactor as a heat source. Useful electrical power output is obtained from an alternator directly coupled to the turbine shaft.

The work presented was performed under a subcontract to Atomics International with the following prime objectives:

a) Select the type of turbine that will best suit the SNAP II requirements.

b) Design, fabricate, and test such a turbine in order to evaluate its performance at both design-point and off-design operating conditions.

c) Determine areas of possible improvement.

A preliminary analysis conducted on various types of turbines has indicated that a two stage, axial flow, full admission turbine with some reaction across the second stage would best suit the SNAP II requirements.

Experimental results have confirmed the turbine design approach and have indicated an over-all turbine efficiency of 46% at the design point with a corresponding power output of 2.58 KW. Turbine performance improvement to equal or exceed the 55% efficiency objective shall be realized by design refinements determined from the results of the turbine tests.

1.0 INTRODUCTION

The SNAP II auxiliary power unit for 3 KW of electrical output consists of an Atomics International Reactor Heat Source and a Thompson Ramo Wooldridge power conversion system. The power conversion system is a mercury Rankine engine which is composed of a mercury boiler heated by a sodium heat transfer loop, an axial flow impulse turbine which extracts energy from the superheated mercury vapor, a condenser which returns the vapor to a liquid state and a mercury pump which returns the condensate to the boiler. The turbine directly drives the alternator, the mercury pump, and a permanent magnet induction sodium pump which is designed to circulate the sodium between the mercury boiler and the reactor.

Thompson Ramo Wooldridge has been actively engaged in development of high performance turbines from the inception of jet aircraft. Small turbine technology has had particular emphasis in the development of air turbine driven fuel pumps. Small turbine design techniques were further advanced with the development of chemical auxiliary power units for the Terrier, Navaho, Bullpup, and Bomarc missiles.

Background information on mercury turbines was obtained from the SNAP I program. The lower power SNAP I system utilizes a similar mercury Rankine engine with an isotope heat source instead of a reactor. In the SNAP I program, both axial flow and regenerative type turbines were analyzed and tested with air and steam as the working medium. SNAP I testing on axial flow turbines utilizing mercury as the working fluid was initiated in July, 1958. All available information that applied to the SNAP II turbine was incorporated in the design shortly thereafter.

Digital computer programs which were developed from many years of small turbine experience were also utilized in the design and test analysis of the SNAP II axial flow turbine performance.

Precision manufacturing of the individual nozzle and wheel blade profiles represents a major accomplishment in small turbine fabrication. Individual blade fabrication techniques allow for a hardened blade design and also allow for high production, low cost manufacturing.

Selection of the cycle condictions which establish the SNAP II turbine operating requirements are reported in the SNAP II Topical Report #1 titled "Design Point Determination" (Thompson Ramo Wooldridge Engineering Report No. 3619 - Document AE-61(A).

The following sections of this report describe the selection and design of the SNAP II two stage, axial flow turbine. Also, the test apparatus and test analysis for this turbine are described.

2.0 TURBINE DESIGN

2.1 Turbine Selection

The turbine type selected for this application is basically a two stage axial flow impulse full admission machine modified by the addition of some reaction in the last stage. The selection of this type of turbine was the result of evaluation of the following turbine types.

2.1.1 Axial Flow Impulse Turbine

In the axial flow impulse turbine, the entire available expansion takes place in the stationary nozzles. The high velocity gases are then admitted into the rotating blades where the high kinetic energy of the impinging jet is converted into mechanical energy by changing its direction.

Advantages are listed below:

a) No pressure drop exists across the rotor, thus axial thrust is small, and bearing loads are minimized.

b) In addition, the constant pressure blading minimizes leakage losses, a major loss consideration in very small turbines.

c) Impulse turbine design is well advanced since considerable work has been done towards improving and accurately predicting performance.

The pressure ratio across a single stage is limited by three factors:

a) Compression shocks and expansion waves occurring downstream of the nozzles limit exit velocities to approximately Mach 1.3 for straight back nozzles. These shocks cause disturbances in the flow pattern and introduce high losses.

b) Relative velocity approaching the rotor should be kept below a Mach number of .85 to avoid normal shocks in the blade passage which may lead to separation on the suction side of the blade.

c) Too large an expansion of a condensible working fluid results in excessive moisture and consequent turbine erosion.

Pressure ratio is thus limited to approximately 4:1 per stage for optimum nozzle efficiency.

2.1.2 Axial Flow Reaction Turbine

In the axial flow reaction type turbine, part of the pressure drop occurs in the nozzle and the remainder in the rotor. Efficiency is at a peak when half of the energy release is accomplished in the blading. The advantages are as follows:

a) All blade contours are such as to give converging channels, resulting in a pressure gradient that will suppress the boundary layer. Frictional losses are thus reduced.

b) For this type of turbine, the peak efficiency is relatively insensitive to variations in u/C (rotor tangential velocity to nozzle exit velocity ratio). This fact allows a wider latitude in the choice of variables.

c) Reaction type turbine development is in a well-advanced state.

Disadvantages include:

a) Close rotor tip clearances are necessary to minimize tip leakage because of the pressure gradient across the rotor blade.

b) Axial thrust exists because of the pressure gradient across the rotor. This force increases bearing sizes and cooling problems.

c) Full admission nozzles must be used in order to sustain a pressure drop across the rotor blades.

2.1.3 Pure Reaction Turbine

The pure reaction turbine is a radial outflow machine where flow enters the center of the wheel and flows to nozzles situated along the periphery. The machine is a high flow device which could be overcome by multistaging, but diffuser and disc-drag losses drop the efficiency considerably.

2.1.4 Radial Inflow (or Outflow) Turbine

In the radial inflow turbine, fluid enters the periphery, travels toward the center and is exhausted there. As it passes through the rotor blades, energy is transferred to the rotor by virtue of changing velocity.

Advantages are:

a) Rotor is of simple construction and rugged.

b) Efficiencies are high for proper specific speeds.

Disadvantages are:

a) Pressure ratio is limited because of specific volume increase as fluid passes through blades while discharge area is limited.

b) Leakage losses are high.

c) Multistaging is awkward and inefficient. (SNAP II specific speed would require multistaging.)

d) Excessive windage and disc friction losses.

2.1.5 Drag (or Regenerative) Turbine

In drag (or regenerative) turbines the flow of fluid repeatedly enters and discharges from the same wheel. The fluid enters along the periphery and continues through the wheel until it is exhausted. The effect of multistaging is thus accomplished in a single rotor.

Advantages are:

a) The multistaging effect makes high pressure drops feasible in a single wheel.

b) Single wheel construction simplifies fabrication.

c) The turbine can operate on less superheat because flow is kept dry by frictional reheating and moisture is separated by centrifugal effects.

d) High efficiencies do not promote erosion damage. This is due to the wheel's ability to operate in a wet environment.

Disadvantages are:

a) Considerable research and development must be undertaken before a satisfactory regenerative turbine could be designed.

b) Preliminary analysis and test have predicted a maximum efficiency of 30% which is considerably lower than could be obtained with a conventional axial flow turbine.

In summary, the selection was based upon:

1. Highest predictable efficiency.
2. Compact mechanical design.
3. Compatibility with the bearing load capacity.
4. Good assurance of extended life capability.
5. Reasonable, though not minimum, fabrication costs.

2.2 Specifications

The SNAP II turbine design was based on design-point conditions illustrated in Table I (a) below:

TABLE I
TURBINE DESIGN POINT OPERATING CONDITIONS & PARAMETERS

	(a)	(b)
Rotational Speed, rpm	40,000	40,000
Inlet Total Pressure, psia	100	105
Inlet Total Temperature, °F	1,150	1,150
Exit Static Pressure, psia	6.2	6.5
Required Power Output, KW	4.86	5.16

Later system analysis established slightly increased power output requirements for the turbine. Thereafter, operating conditions were changed to those shown in Table I (b) while the original turbine design was retained. These changes in operating conditions had the effect of a five percent increase in mass flow with substantially no change in the velocity diagrams.

2.3 Design Procedure and Assumptions

2.3.1 Design Methods

In the design of the SNAP II turbine, methods and procedures previously developed for the design of small output turbines were used. This design method has included such normally secondary losses as leakage and heat which, for small output turbines, are of primary importance.

2.3.2 Design Assumptions

a) Mercury vapor properties were based on data obtained from the Bureau of Standards.

b) On the basis of known steam technology, an analogous Wilson Line was assumed at the four percent moisture line. The Wilson Line is defined as an experimentally observed suppressed saturation line at which nucleation and condensation of liquid particles begin. Vapor state points between the saturated vapor line and the four percent Wilson Line were assumed to be supersaturated. Supersaturated vapor is defined as vapor that has been cooled below the saturation temperature corresponding to its pressure.

c) Critical pressure ratios in the nozzles were calculated from perfect gas equations.

2.4 Turbine Design Parameters and Dimensions

Using the design specifications with the assumptions and procedures cited in Sections 2.2 and 2.3, the turbine geometric and aero-thermodynamic parameters were determined as listed in Tables II and III. New fabrication procedures for blades and nozzles introduced certain small tolerance deviations which, due to the time element involved, were not corrected. Thus, the turbine dimensions as fabricated are as shown in Table II (b). In Figure 1a side views of the fabricated stator and rotor assemblies are shown.

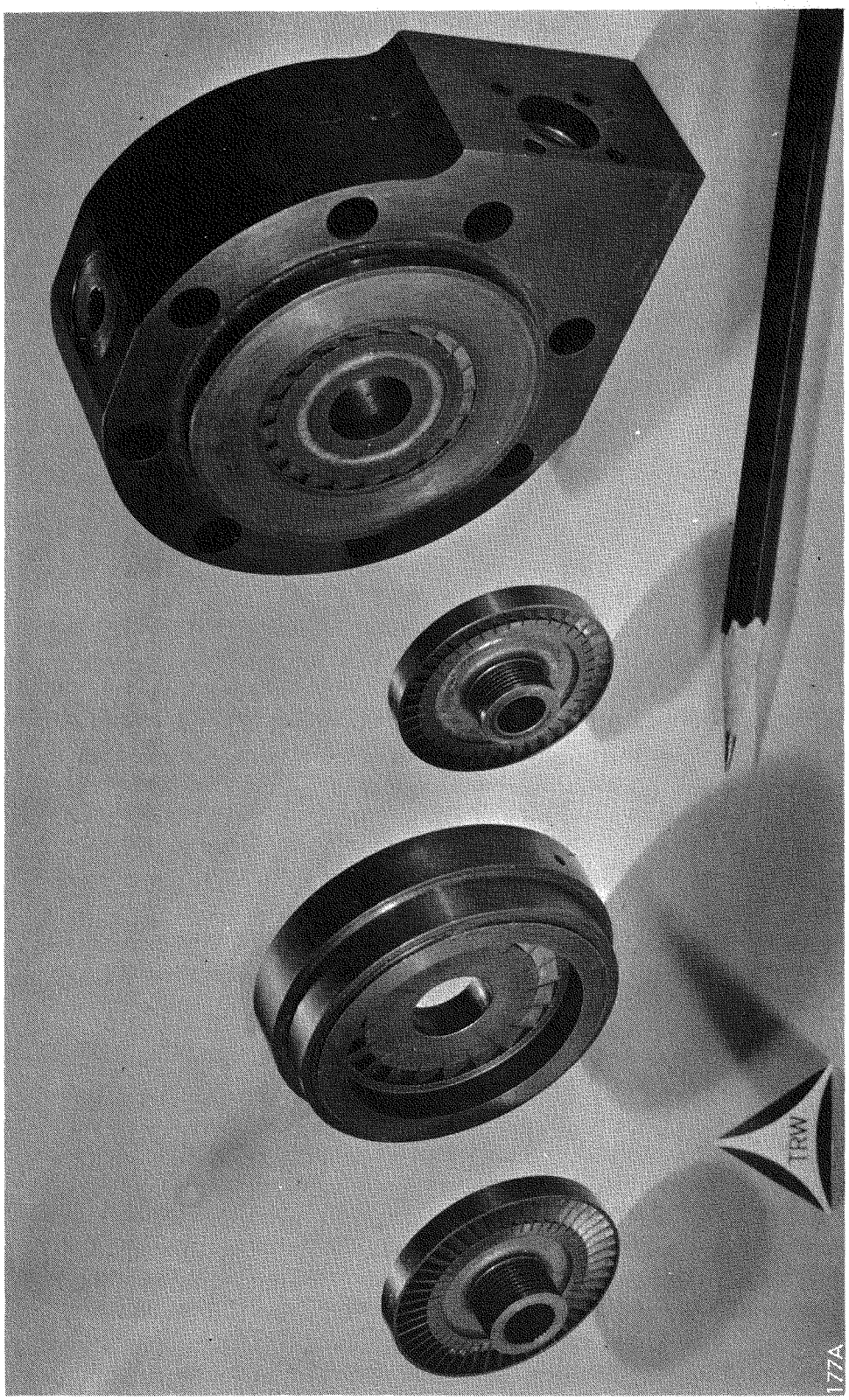

FIGURE 1a TURBINE TEST ROTORS AND NOZZLES

TABLE II
TURBINE GEOMETRIC PARAMETERS

GEOMETRIC PARAMETERS		(a) DESIGN DIMENSIONS		(b) FABRICATION DIMENSIONS	
		1st STAGE	2nd STAGE	1st STAGE	2nd STAGE
Nozzle Pitch Diameter,	D_{m1}, in	1.4	1.4	1.399	1.401
Rotor Pitch Diameter,	D_{m2}, in	1.4	1.4	1.398	1.399
Nozzle Height,	ℓ_1, in	.0883	.156	.08835	.157
Rotor Blade Height,	ℓ_2, in	.1155	.2160	.11425	.2140
Nozzle Axial Chord,	b_{x_1}, in	.20	.28	.20	.28
Rotor Axial Chord,	b_{x_2}, in	.2	.2	.2	.2
Nozzle Inlet Angle,	α_o	138°	49°	138°	49°
Nozzle Exit Angle	α_1	15°	20°	15°	20°
Rotor Inlet Angle,	β_1	27°	36°	27°	36°
Rotor Exit Angle	β_2	24°	32°	24°	32°
Number of Nozzles,	N_n	20	20	20	20
Nozzle Throat Width (gaging),	λ_1 in	.05092	.07021	.04300	.0685
Rotor Exit Throat Width (gaging),	λ_2 in	.04087	.04959	.04087	.04900
Nozzle Exit Actual Area,	F_1, in^2	.08992	.21906	.07598	.21510
Rotor Exit Actual Area,	F_2, in^2	.1841	.50344	.1821	.49284
Labyrinth Seal Clearance,	Δ_d in	.005	.005	.0063	.0063
Shroud Radial Clearance,	c, in	.005	.005	.0093	.0093
Number of Blades,	N_b	39	47	39	47

TABLE III

TURBINE DESIGN-POINT AERO THERMODYNAMIC PARAMETERS

THERMODYNAMIC PARAMETERS			1st STAGE	2nd STAGE
Inlet Scroll Velocity	C_o	ft/sec	160	-----
Inlet Nozzle Velocity	C_o	ft/sec	160	243
Nozzle Exit Velocity	C_1	ft/sec	828	715.0
Turbine Flow	W_f	lb/min	16	16
Nozzle Inlet Total Pressure	Poo	psia	100	33.33
Nozzle Static Exit Pressure	P_1	psia	30	9.2
Nozzle Exit Moisture	X_1	%	3	5.1
Rotor Inlet Velocity	W_1	ft/sec	596.5	494.53
Rotor Exit Velocity	W_2	ft/sec	458.8	554.60
Rotor Exit Static Pressure	P_2	psia	30	6.2
Rotor Tangential Velocity	u	ft/sec	244.3	244.3
Scroll Exit Velocity	C_4	ft/sec	-----	450
Nozzle Inlet Total Enthalpy	hoo	Btu/lb	159.3	150.265
Nozzle Exit Static Enthalpy	h_1	Btu/lb	145.61	139.68
Rotor Inlet Total Enthalpy	h_{01}	Btu/lb	152.71	144.940
Rotor Inlet Total Pressure	P_{01}	Btu/lb	54	14.8
Rotor Exit Static Enthalpy	h_2	Btu/lb	148.50	139.19
Stage Power Output	HP	hp	3.408	3.199
Rotor Exit Moisture	X	%	.25	5

3.0 TURBINE TEST PROGRAM OBJECTIVES

The object of this series of tests was to:

1. Establish and verify the turbine performance at both the design and off-design points.

2. Compare and correlate test data with calculated data in order to substantiate the loss system used in conjunction with turbine design and off-design analytical procedures.

3. Determine areas for possible improvement.

4. Verify design assumptions on which TTP turbine was based, particularly those of supersaturation and thermal losses.

Figures 1b and 1c show the turbine test package.

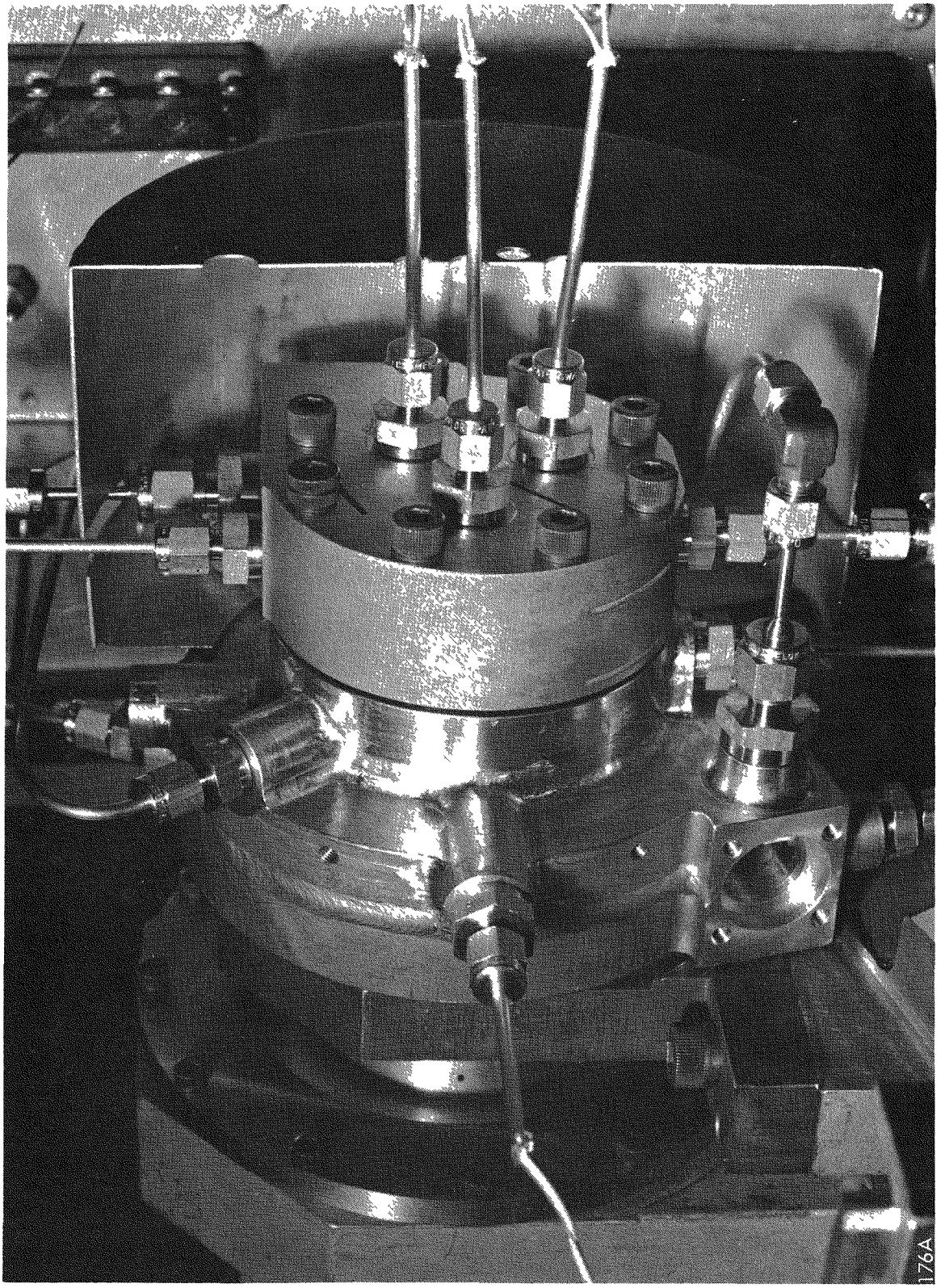

FIGURE 1b TURBINE TEST PACKAGE - TURBINE END

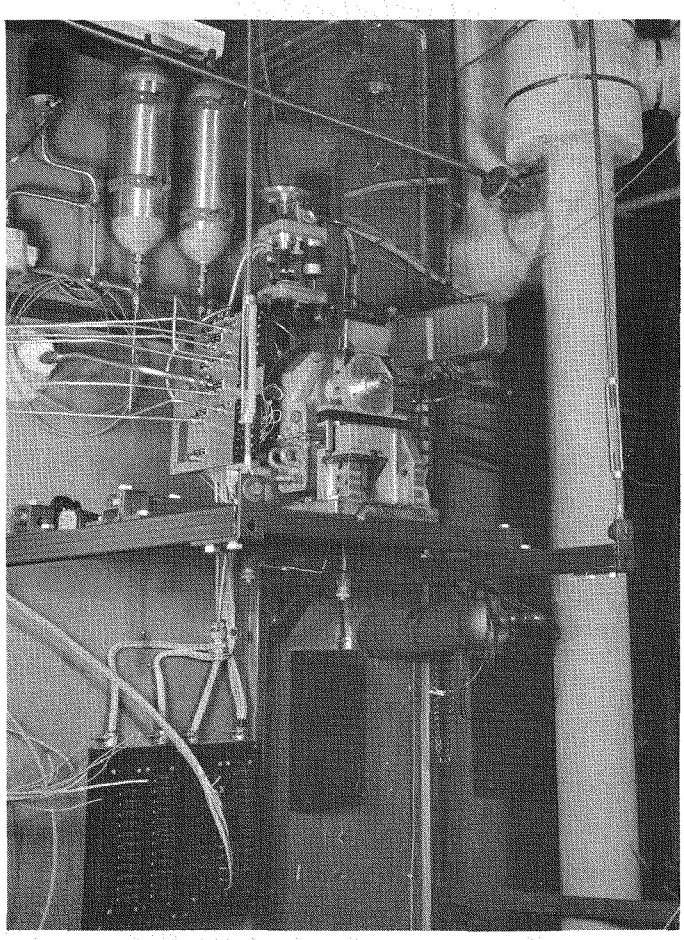

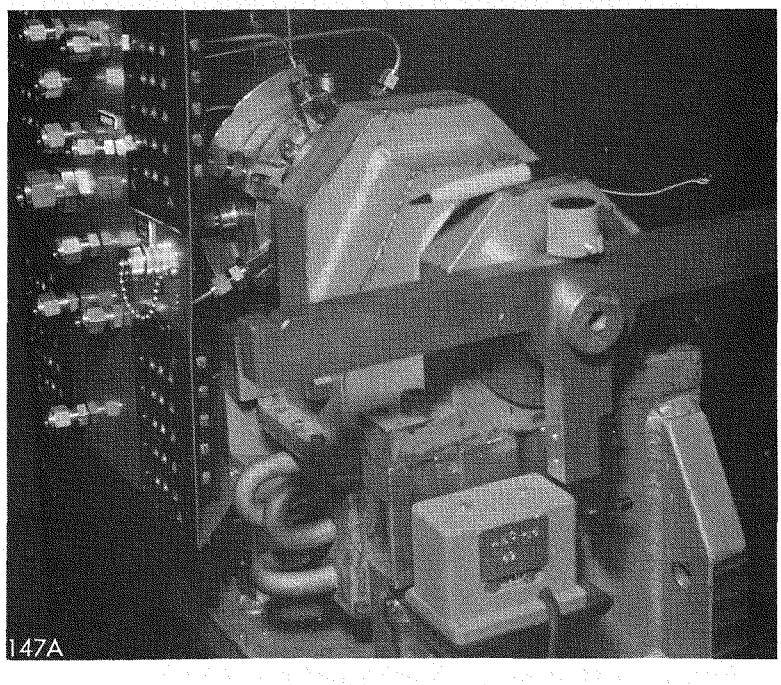

TURBINE DYNAMOMETER IN TEST RIG WITH INSERT SHOWING TURBINE AND HOUSING

FIGURE 1c

4.0 METHOD OF DATA ANALYSIS

4.1 Data Reduction

Raw data from recording tape was reduced and corrected for all known systematic errors. A probable error band has also been defined for each parameter, as shown in Section 5.2.1.

4.2 Calculation of Turbine Parameters

Thermodynamic parameters were then calculated from corrected data, such as $\frac{W_f \sqrt{Too}}{Poo}$, $\frac{HP}{Poo \times \sqrt{Too}}$, etc. These parameters were plotted to establish empirical trends and correlations that exist between the above mentioned characteristic parameters. From these plots, interrelation of various parameters was checked so that both energy and continuity equations were satisfied and in complete agreement with each other.

4.3 Statistical Analysis and Correction

Scatter and discrepancies that might exist in the parametric plots of Section 4.2 were then corrected by statistical methods. Experimental points that were obviously erroneous due to possible instrument malfunctioning were separated out. Final turbine performance parameters were replotted and presented as shown in Figures 2 to 8.

4.4 IBM Experimental Data Simulation

Corrected data was simulated by means of the IBM 650 turbine off-design program as follows: Given turbine actual fabrication dimensions, and such parameters of a particular run as initial pressure and temperature, rotational speed, exit static pressure, total exit temperature and pressure, and power output, the calculation proceeded as follows: Initial conditions, RPM, and static exit pressure along with turbine geometry were read into the machine by means of punched cards. The IBM machine calculated the remaining exit conditions and power output through successive iterations. Calculated parameters were then compared with the experimental values to check for possible discrepancies. If a discrepancy existed between the experimental parameters and the corresponding calculated values, the appropriate loss coefficients built in the program were changed until complete agreement existed between the parameters under comparison.

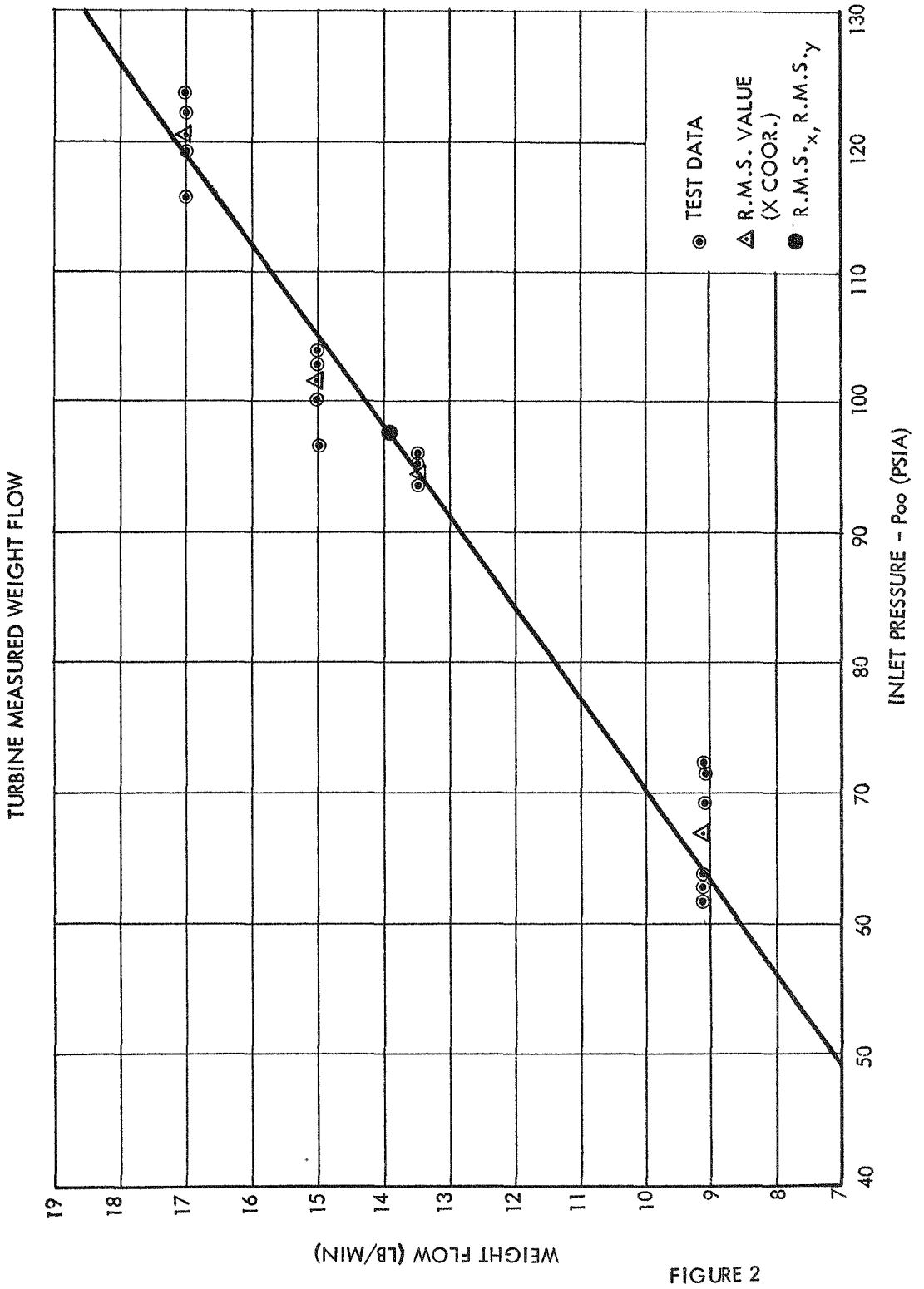
TURBINE MEASURED WEIGHT FLOW
WEIGHT FLOW (LB/MIN)
INLET PRESSURE - Poo (PSIA)
TEST DATA
R.M.S. VALUE (X COOR.)
R.M.S.x, R.M.S.y
19
18
17
16
15
14
13
12
11
10
9
8
7
40
50
60
70
80
90
100
110
120
130

FIGURE 2

TURBINE CALCULATED WEIGHT FLOW FROM EXPERIMENTAL DATA

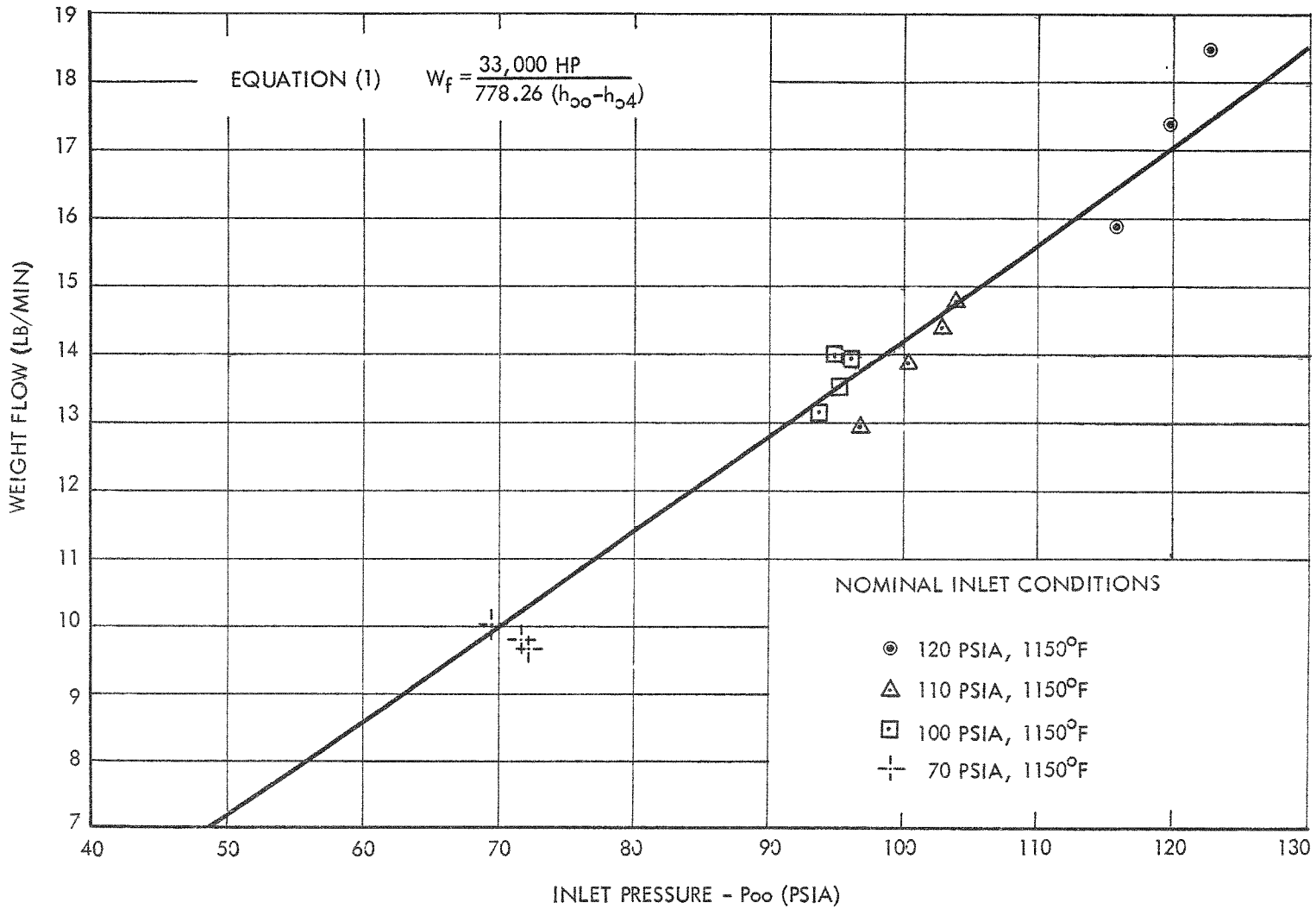

FIGURE 3

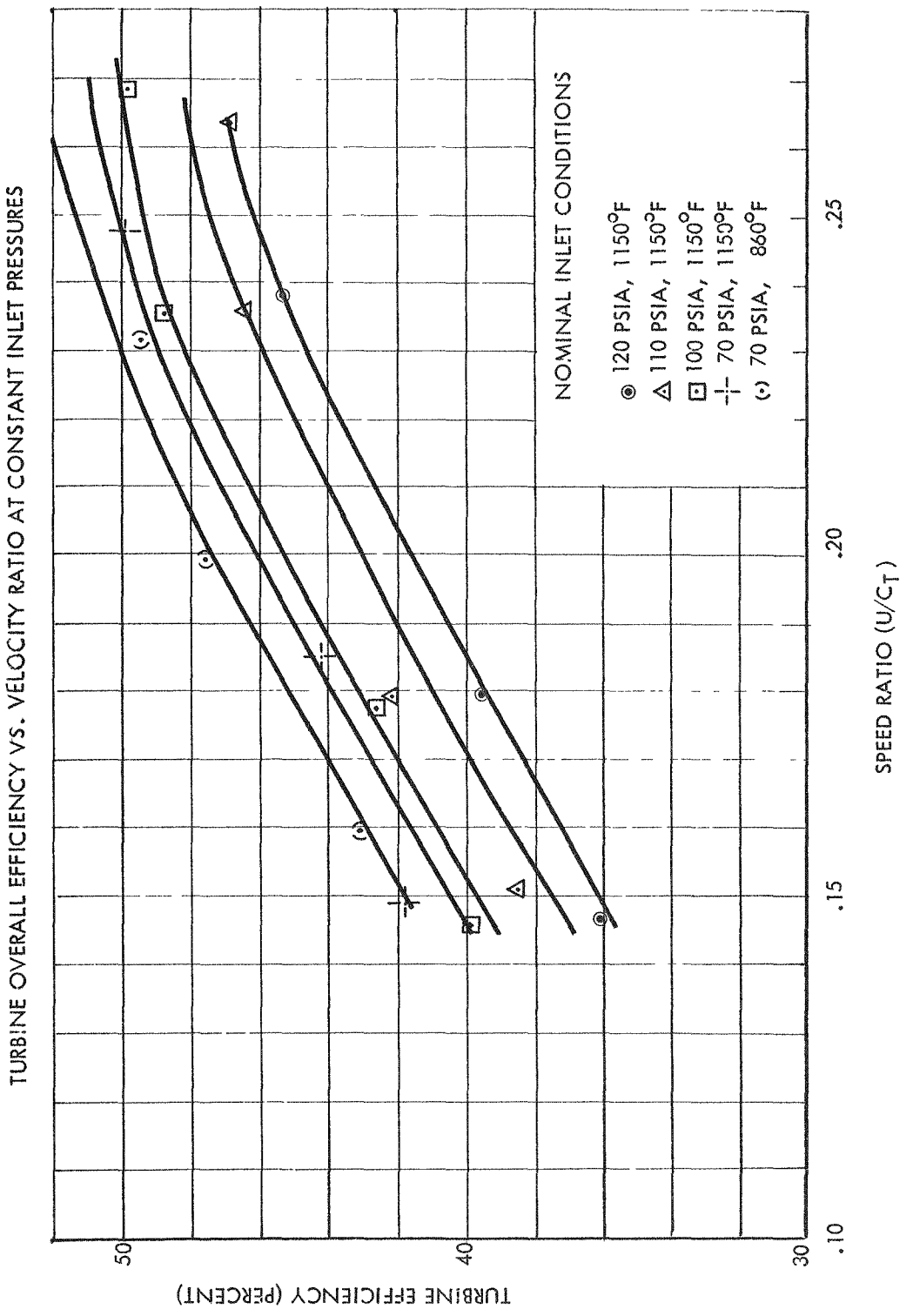
TURBINE OVERALL EFFICIENCY VS. VELOCITY RATIO AT CONSTANT INLET PRESSURES
NOMINAL INLET CONDITIONS
120 PSIA, 1150°F
110 PSIA, 1150°F
100 PSIA, 1150°F
70 PSIA, 1150°F
70 PSIA, 860°F
TURBINE EFFICIENCY (PERCENT)
50
40
30
.10
.15
.20
.25
SPEED RATIO (U/CT)

FIGURE 4

TURBINE HORSEPOWER VS. VELOCITY RATIO AT CONSTANT INLET PRESSURE

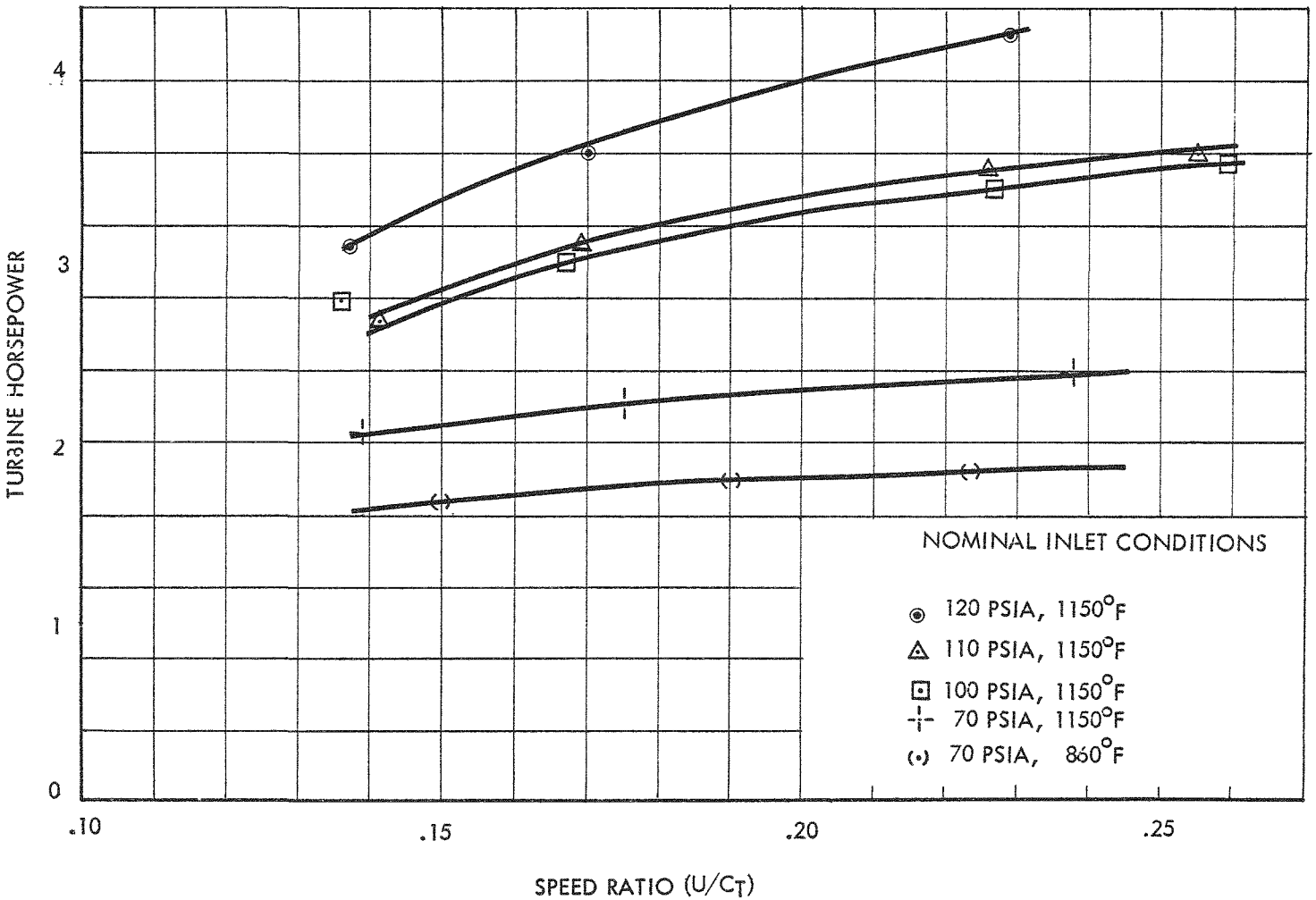

FIGURE 5

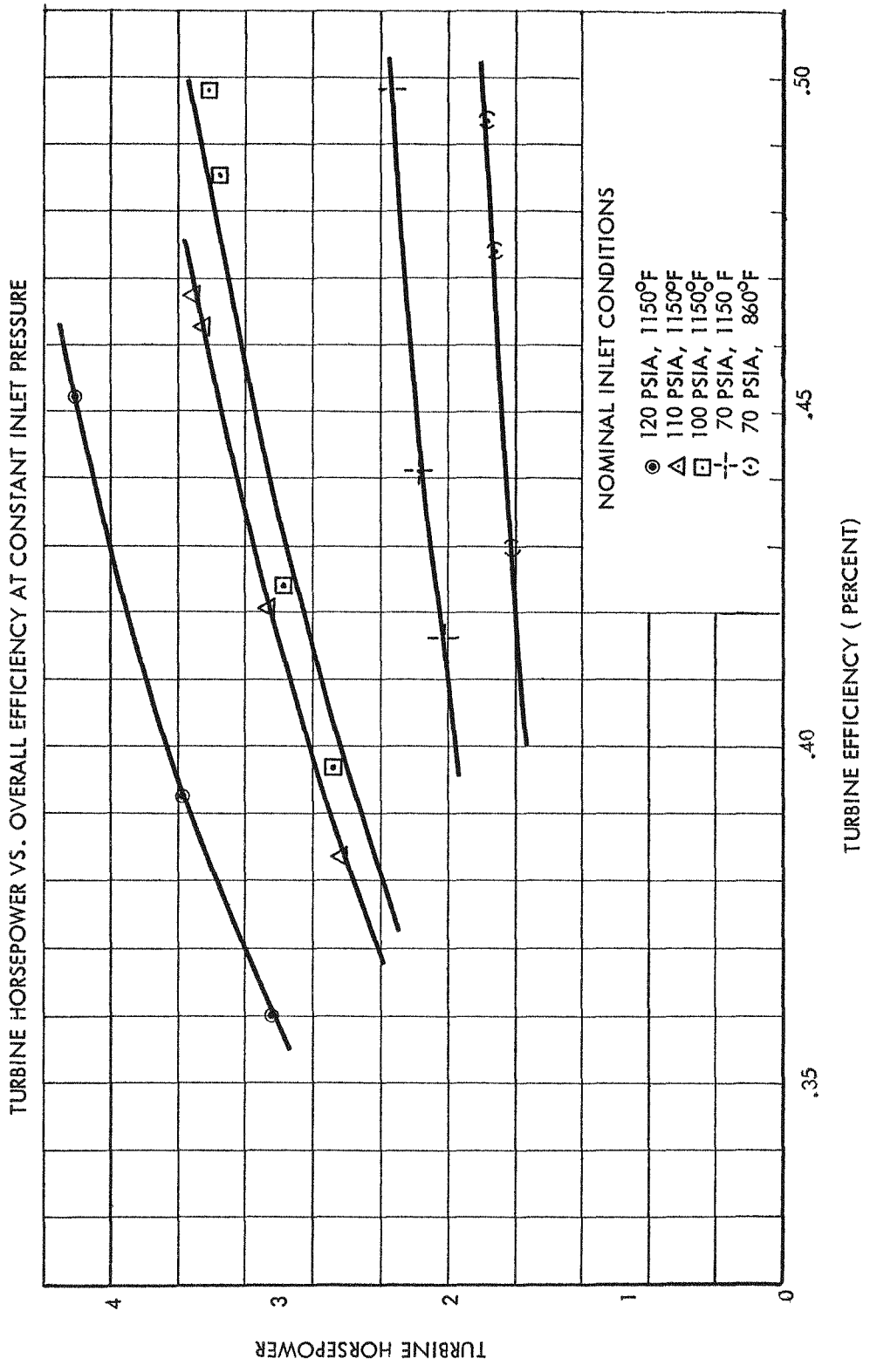
TURBINE HORSEPOWER VS. OVERALL EFFICIENCY AT CONSTANT INLET PRESSURE
NOMINAL INLET CONDITIONS
120 PSIA, 1150°F
110 PSIA, 1150°F
100 PSIA, 1150°F
70 PSIA, 1150 F
70 PSIA, 860°F
TURBINE HORSEPOWER
0
1
2
3
4
.35
.40
.45
.50
TURBINE EFFICIENCY (PERCENT)

FIGURE 6

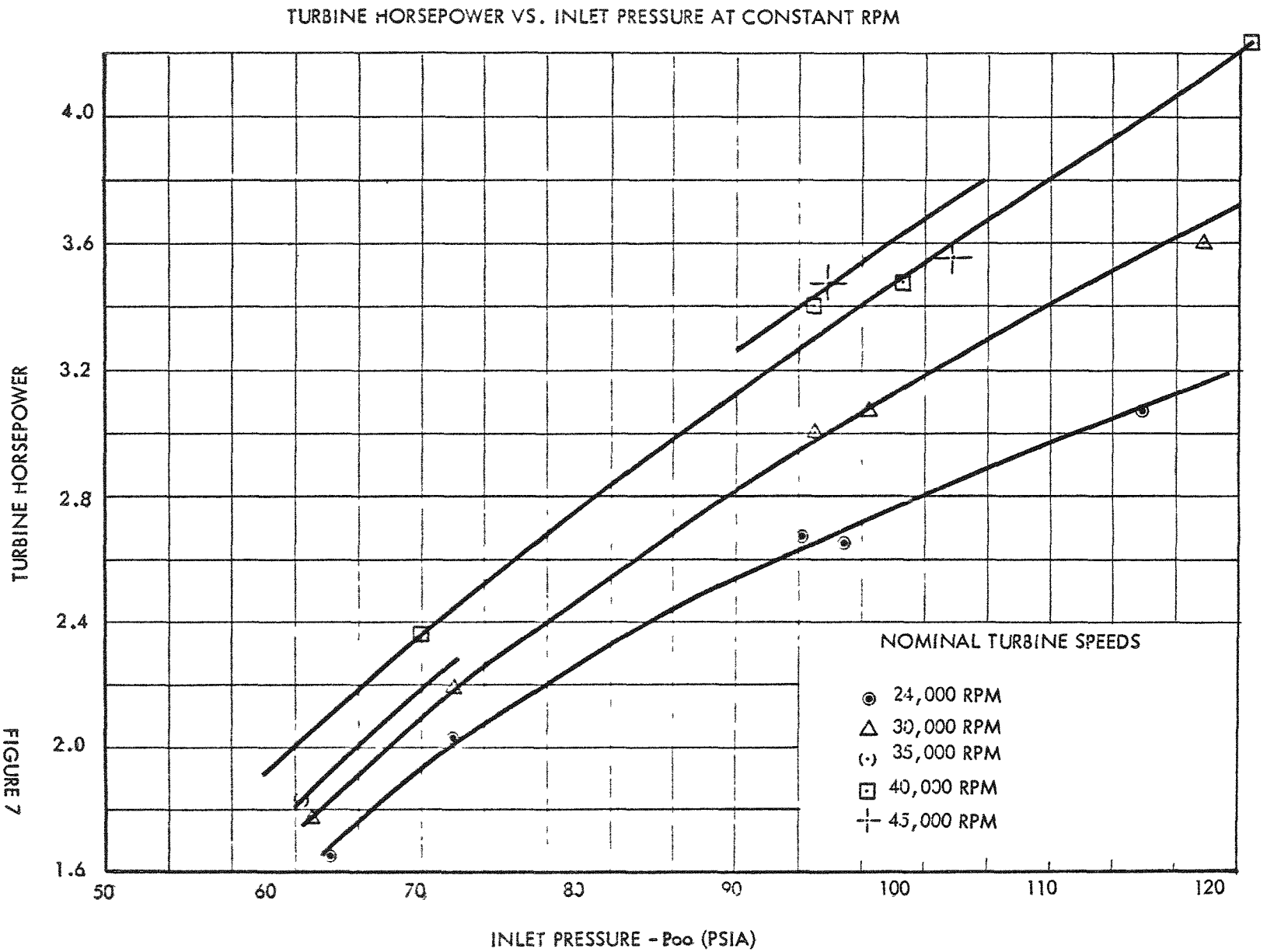
TURBINE HORSEPOWER VS. INLET PRESSURE AT CONSTANT RPM
TURBINE HORSEPOWER
4.0
3.6
3.2
2.8
2.4
2.0
1.6
50
60
70
80
90
100
110
120
INLET PRESSURE - Poa (PSIA)
NOMINAL TURBINE SPEEDS
24,000 RPM
30,000 RPM
35,000 RPM
40,000 RPM
45,000 RPM

FIGURE 7

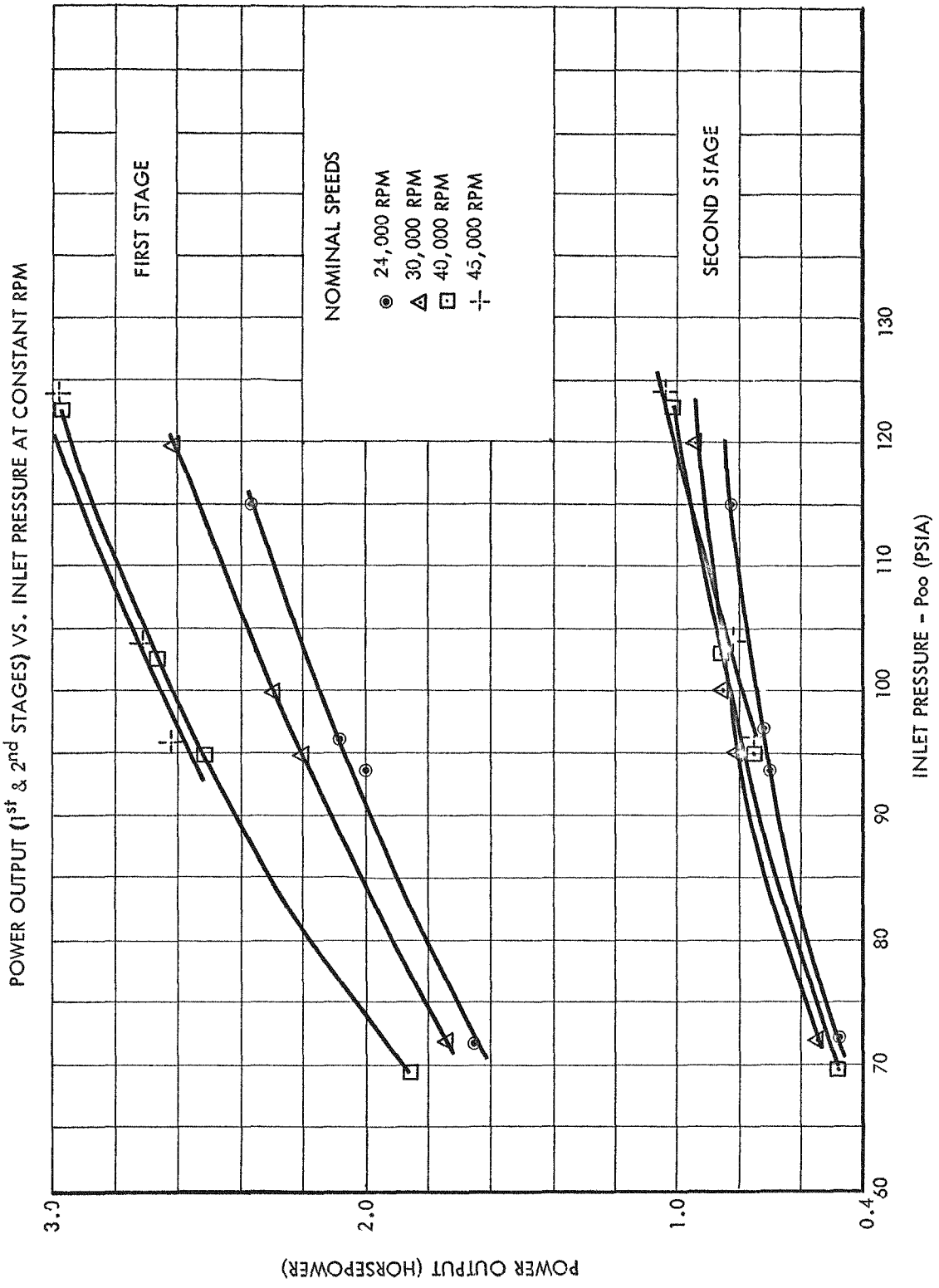
POWER OUTPUT (1st & 2nd STAGES) VS. INLET PRESSURE AT CONSTANT RPM
FIRST STAGE
SECOND STAGE
NOMINAL SPEEDS
24,000 RPM
30,000 RPM
40,000 RPM
45,000 RPM
POWER OUTPUT (HORSEPOWER)
INLET PRESSURE - Poo (PSIA)
3.0
2.0
1.0
0.4
60
70
80
90
100
110
120
130

FIGURE 8

The new loss coefficients were then compared with the ones originally used to design the turbine and any corrections were transferred to the IBM turbine design program to be utilized towards new turbine designs.

4.5 Turbine Performance Presentation

The best method of presenting turbine data is through a series of curves showing the relationships of the variables, speed (N), inlet pressure (Poo), inlet temperature (Too), exhaust pressure (P_4), efficiency (η_t), and weight flow (W_f). The desired curves are as follows:

1. $\dfrac{HP}{Poo\sqrt{Too}}$ vs. $\dfrac{P_4}{Poo}$ at constant $\dfrac{N}{\sqrt{Too}}$ ratios

2. $\dfrac{W_f\sqrt{Too}}{Poo}$ vs. $\dfrac{P_4}{Poo}$ at constant $\dfrac{N}{\sqrt{Too}}$ ratios

3. η_t vs. $\dfrac{U}{C_t}$

Curves used to describe the SNAP II turbine data are similar to those used in turbo-machinery. Various parameters used in presentation of data were obtained from raw experimental data and were calculated as indicated in Section 9.1 of this report.

5.0 DISCUSSION OF TEST RESULTS

5.1 Experimental Turbine Performance Curves

In Figures 2 through 8 the turbine performance curves, obtained at nearly constant pressure ratio across the turbine, are presented. As discussed in Section 5.2, choking of the exit scroll prevented variation of the pressure ratio and presentation of the data as proposed in Section 4.5. Hence, the method of describing performance was altered somewhat to bring out some of the important turbine characteristics.

Figures 2 and 3 establish the weight flow through the turbine, as obtained by two different methods, at various initial pressures and approximately constant inlet temperature. Figure 2 presents the weight flow as measured and corrected for RMS values of both co-ordinates, while Figure 3 gives the weight flow as calculated from Equation (1) where HP, hoo, and h_{o4} are experimentally obtained values for a particular run. Neglecting external heat losses,

$$W_f = \frac{33{,}000\ HP}{778.26\ (hoo - h_{o4})} \qquad \text{Equation (1)}$$

Results of this method are slightly incorrect in that HP measured by the dynamometer does not include disc friction and windage losses of the rotating parts. Nevertheless, the small magnitude of calculated disc losses may justify the use of Equation (1) for checking purposes.

Figures 4 through 7 illustrate the variation of turbine efficiency and horsepower with rim velocity ratio u/C_t and initial pressure Poo. For nomenclature, see List of Symbols in Section 9.2. As indicated, turbine efficiency η_t increases with decreasing inlet pressure Poo and increasing rim velocity ratio u/C_t or rotational speed N. The turbine power output increases with increasing inlet pressure Poo and speed N. The above phenomena may be explained by Equations (7) and (8) below. These relations have been derived in Section 9.3 from the fundamental relations that exist between the parameters HP, η_t, Δh_j, N and W_f.

$$\eta_t = \frac{a_9 N}{\sqrt{Poo}} \qquad \text{Equation (7)}$$

$$HP = a_{10} N\ Poo^{1.5} \qquad \text{Equation (8)}$$

Equations (7) and (8) show that HP is directly proportional to the rotational speed N and initial pressure Poo while the over-all turbine efficiency η_t is proportional to N and inversely proportional to Poo.

These equations are based on the following assumptions:

a) Constant inlet temperature, Too

b) Constant pressure ratio across the turbine

c) Constant turbine geometery

d) Linear relationship of η_t vs. u/C_t below peak efficiency

Figure 8 presents the power output variation of the individual stages with turbine initial pressure Poo and at constant RPM. It appears that both stages reach peak performance at an inlet pressure of approximately 130 psia with the first stage supplying 74% of the total turbine output. Calculated stage and turbine over-all outputs are listed in Table IV along with dynamometer measured values. Calculated values are based on experimental state points and show a maximum deviation of 5.5% when compared to the dynamometer measured values.

5.2 Over-all Data Discussion

With pressure and temperature probes located as illustrated in the schematic diagram of Figure 9, initial, interstage, and exhaust state points were recorded by both visual and electrical means. After reducing and correcting data points for all possible errors, they were tabulated as shown in Section 9.1.

Proceeding with data evaluation methods of Section 4.0, each of the experimental data points was examined for possible instrument or positional errors. This investigation yielded the following results:

1) Inlet Scroll

Continuity and energy equations yielded scroll average velocities of the order of 160 ft/sec with a corresponding pressure drop of .1 psi. Such pressure drop was neglected and nozzle inlet pressure was assumed equal to the scroll inlet pressure Poo.

Four thermocouples placed on the inside periphery of the scroll recorded the temperature distribution and heat losses from the fluid to the surrounding wall. Conduction effects were discovered

SCHEMATIC DIAGRAM SHOWING LOCATIONS OF TEMPERATURE & PRESSURE PROBES

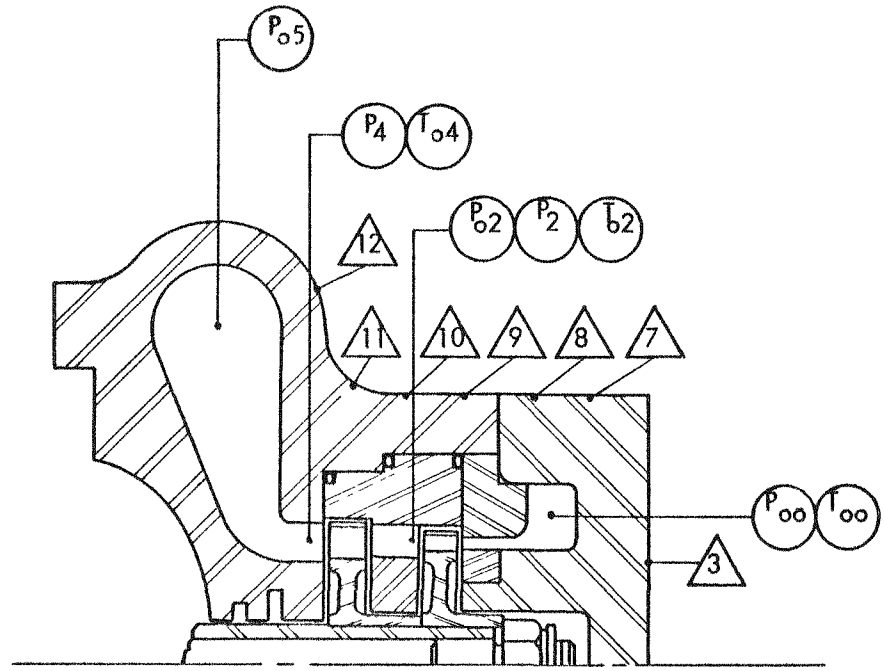

△	SURFACE PROBES
P_{oo}	FIRST STAGE NOZZLE INLET-TOTAL
T_{oo}	FIRST STAGE NOZZLE INLET-TOTAL
P_{o2}	SECOND STAGE NOZZLE INLET-TOTAL
P_2	SECOND STAGE NOZZLE INLET- STATIC
T_{o2}	SECOND STAGE NOZZLE INLET-TOTAL
P_4	SECOND STAGE ROTOR DISCHARGE-STATIC
T_{o4}	SECOND STAGE ROTOR DISCHARGE-TOTAL
P_{o5}	TURBINE DISCHARGE DUCT-TOTAL

FIGURE 9

TABLE IV

CALCULATED INDIVIDUAL STAGE AND OVER-ALL TURBINE POWER OUTPUTS BASED ON EXPERIMENTAL DATA

RUN	HP_{1st}	HP_{2nd}	HP_{TS}	HP_{DYN}	$\frac{\Delta HP}{HP_{DYN}}$
1	2.354	.817	3.171	3.046	4.1%
2	2.626	.9184	3.544	3.589	1.25
3	2.992	1.0111	4.003	4.225	5.25
4	2.987	1.0317	4.0187	———	———
5	2.082	.7157	2.7977	2.652	5.49
6	2.293	.8508	3.1438	3.065	2.57
7	2.663	.808	3.5256	3.471	1.57
8	2.718	.819	3.537	3.545	.23
9	2.001	.7089	2.7099	2.675	1.30
10	2.206	.7907	2.977	2.998	.03
11	2.505	.7641	3.269	3.398	3.79
12	2.620	.7473	3.3673	3.462	2.74
13	1.653	.4772	2.1302	2.033	4.781
14	1.733	.5282	2.2612	2.189	3.30
15	1.848	.4697	2.3177	2.346	1.21

Column (1) - First Stage Power Calculated from Experimental State Points

Column (2) - Second Stage Power Calculated from Experimental State Points

Column (3) - Turbine Over-All Power from Summation of (1) & (2)

Column (4) - Dynamometer Turbine Power Output

Column (5) - % Deviation in Turbine Output Between Columns (3) & (4)

in one of the probe readings and the reading was therefore neglected in obtaining the inlet scroll average temperature. For most experimental runs, this temperature was in the superheat region. The average amount of superheat was approximately 250°F as illustrated in Table V.

Existing temperature gradients in the scroll may have introduced peripheral variations in fluid conditions downstream.

2) Interstage

At this station, total temperature $T_{02'}$ and pressure $P_{02'}$ along with static pressure P_2, were recorded. For most experimental runs the T_{02} reading was in the superheat region. Thus, T_{02} and P_{02} were sufficient to define a point on the Mercury Mollier Chart. Referring to the velocity and enthalpy-entropy diagrams of Figure 9a, the first stage rotor exit velocity and flow can be calculated from total and static enthalpies defined by $T_{02'}$ P_{02} and P_2 along with the rotor geometry. Results of flow thus calculated are given in Table VI for several experimental runs. By direct comparison with corresponding measured turbine flow rates, discrepancies as much as +27.3% were discovered. Calculated higher rotor flows indicate that one of the interstage fluid parameters, $T_{02'}$ $P_{02'}$ or P_2, must be erroneous. Varying T_{02} by as much as 100°F corrected the discrepancy by 2%. On the other hand, second stage nozzle weight flows based on P_{02} and T_{02} were in complete agreement with the corresponding flows of the first stage. P_{02} may therefore be assumed correct. Process of elimination indicated that the static pressure, P_2, may be erroneous. From continuity and energy considerations at the rotor exit, the calculated P_2 must be 3-4 psi higher than the actual measured values for the various experimental runs. The position of the pressure probe and the radial velocity component may justify a correction of .5 psi.

To explore all possibilities, $P_{2'}$ $T_{02'}$ P_{02} and W_f, as measured, were assumed correct and the rotor exit angle was calculated in order that continuity and energy equations would apply at this station. The calculated rotor exit flow angle was approximately 20° larger than the rotor exit camber angle. Thus, this approach to the problem could only explain the measured P_2 values by severe separation of the fluid from the exit suction side of the blade. This latter approach was substantiated later by the off-design program in which a nominal separation angle of 20° was assumed.

TURBINE STAGE VELOCITY & ENTHALPY-ENTROPY DIAGRAMS

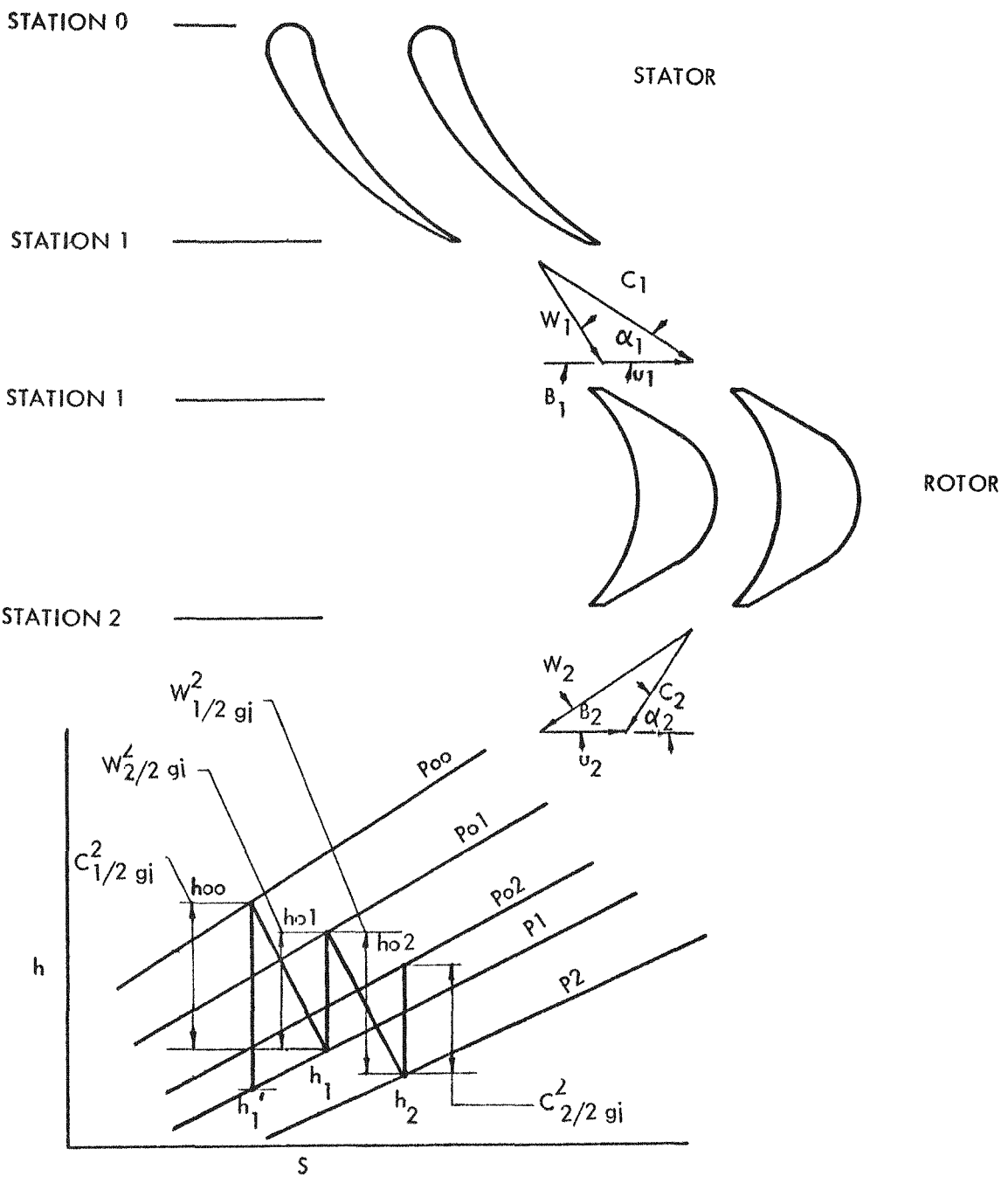

FIGURE 9a

TABLE V

AMOUNT OF SUPERHEAT FOR VARIOUS EXPERIMENTAL RUNS

RUN	Poo psia	Too °F	T_{o4} °F	ΔT (Superheat) °F
1	115.7	1128	930	198
2	119.7	1152	935	217
3	122.7	1156	936	220
4	123.7	1142	938	204
5	96.2	1153	901	252
6	100.2	1157	909	248
7	102.7	1163	912	251
8	103.8	1163	913	250
9	93.8	1140	896	244
10	95.1	1151	900	251
11	94.9	1161	900	261
12	95.7	1158	901	257
13	72.0	1114	864	250
14	71.7	1117	864	253
15	69.5	1123	860	263
16	63.9	841	847	___
17	62.9	802	846	___
18	62.2	807	844	___

TABLE VI

WEIGHT FLOW BASED ON FIRST STAGE ROTOR GEOMETRY AND INTERSTAGE EXPERIMENTAL CONDITIONS

RUN	C_2	W_2	A_{eff}	W_f	W_{fm}	$\frac{W_f - W_{fm}}{W_{fm}}$
	ft/sec	ft/sec	in^2	lb/min	lb/min	%
1	412.65	536.8	.1665	18.65	16.5	+13
2	400.34	553.6	.1657	18.98	17.08	+11
3	360.73	558.1	.1650	19.68	17.5	+12.5
4	339.47	554.0	.1646	19.60	17.64	+11.1
13	401.55	534.8	.1609	13.02	10.22	+27.3
14	395.91	559.7	.1604	11.82	10.18	+16.40
15	328.89	541.1	.1573	11.04	9.86	+12.0

A_{eff} = Effective rotor exit area which has included displacement boundary layer.

W_f = Flow through 1st stage rotor based on interstage experimental data.

W_{fm} = Actual measured flow through the turbine.

For other nomenclature, see List of Symbols or velocity triangle of Figure 9a.

Plotting of Poo versus P_2 in Figure 10 shows a nearly linear variation and that P_2 is insensitive to rotational speed. Until further experimental proof, discrepancy in P_2 may be explained by some leakage taking place in the probe line, separation, probe position, or a combination of all three possibilities.

3) Turbine Exit

A similar situation exists at the exit in that there are static pressure discrepancies at the second stage rotor exit of approximately 1-2 psi.

Two total temperature probes located at this station indicated temperature differences between the two readings by as much as 30-40°F. This fact may substantiate the theory that some peripheral variations in fluid conditions may exist in the turbine. Average probe readings gave a temperature which was in the superheat region with an average superheat of approximately 80°F.

5.2.1 Data Accuracy and Probable Error Estimation

The probable errors of each data reading and calculated values of the turbine parameters are indicated in the following chart.

Data Accuracy and Probable Error Estimation

Pressure Probes	Probable Error %
1. Turbine Inlet Duct - Total	1.73
2. 2nd Stage Nozzle Inlet - Total	2.10
3. 2nd Stage Nozzle Inlet - Static	2.10
4. 2nd Stage Rotor Discharge - Total - Inactive	———
5. 2nd Stage Rotor Discharge - Static	2.10
6. Discharge Duct - Total	2.10
Temperature Probes	
1. Inlet Duct	1.14
2. No. 1 Inlet Scroll	1.14
3. No. 2 Inlet Scroll	1.14
4. No. 3 Inlet Scroll	1.14
5. 2nd Stage Nozzle Inlet	1.14

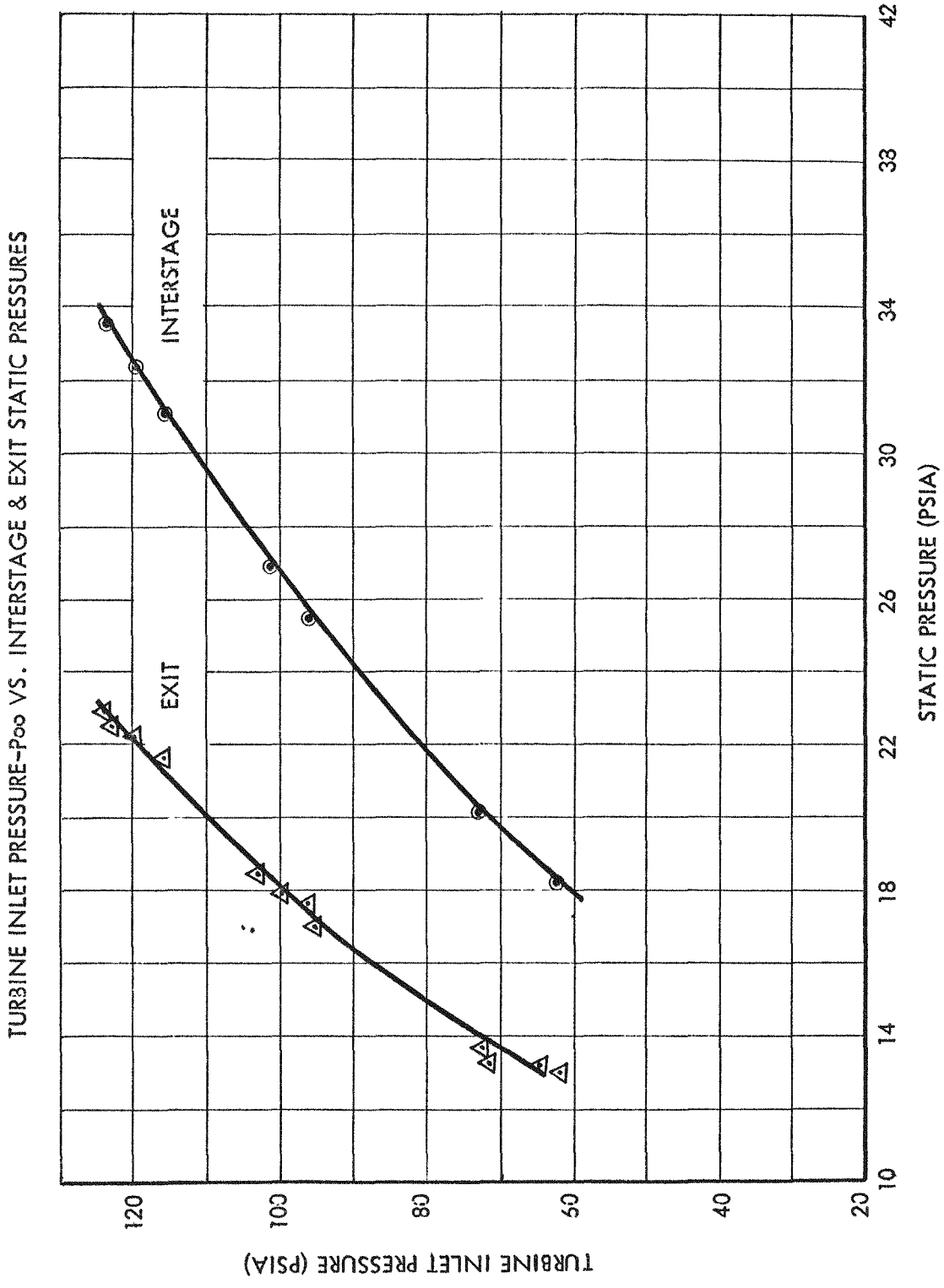
TURBINE INLET PRESSURE-Poo VS. INTERSTAGE & EXIT STATIC PRESSURES
INTERSTAGE
EXIT
TURBINE INLET PRESSURE (PSIA)
120
100
80
60
40
20
STATIC PRESSURE (PSIA)
10
14
18
22
26
30
34
38
42

FIGURE 10

6. 2nd Stage Rotor Discharge No. 1	1.14
7. 2nd Stage Rotor Discharge No. 2	1.14
8. Discharge Duct	1.14
Speed	.77
Torque	1.57
Flow @ 9.1 lb/min	7.86
13.5 "	6.30
15.0 "	5.94
17.0 "	5.55

Data Point or Calculated Value	Probable Error %	Data Point or Calculated Value	Probable Error %
N (RPM)	0.77	W_f (max.)	7.86
Load	1.57	$W_f \Delta h$	9.91
Torque	1.57	$HP/W_f \Delta h$	12.25
HP	2.34	η_t	12.25
Poo	1.73	u	0.77
Too	1.14	$t \Delta h$	14.30
$\sqrt{Too}$	0.57	C_t	2.05
$Poo\sqrt{Too}$	2.30	u/C_t	2.82
$HP/Poo\sqrt{Too}$	4.64	P_4/Poo	3.83
P_4	2.10	N/Too	1.34
hoo	___*		
h_4	___*		
Δh **	2.05		

*Error in h - In the vapor region, the value of h is, for all purposes, a function of temperature alone. The chart plotting and readout error in this range can be considered negligible. Therefore, at a temperature of say 1100°F, the probable error is 1.14% or equal to approximately .21 Btu/lb. This is a probable error in h of $\frac{.21}{158} = .133\%$.

In the wet region, h_4, h'_1 etc., are determined from an isentropic line and a pressure intercept. The pressure being in the range of 13 to 23 psia and the probable error in the pressure being 2.1% would give a maximum error in h of approximately .2 $\frac{Btu}{lb}$. This is a probable error of $\frac{.2}{135} \times 100 = .148\%$. Both errors are negligible.

**Error in Δh - Probable errors of h in the vapor and wet regions are roughly .21 and .20 $\frac{Btu}{lb}$ or .41 Btu/lb. Average $\Delta h = 20 \frac{Btu}{lb}$, therefore the probable error would be

$$\frac{.41}{20} \times 100 = 2.05\%.$$

5.2.2 Turbine Performance at the Design Point

In Table VII calculated and experimentally obtained turbine design-point performances are presented. Experimental performance was taken at inlet operating conditions which approximately correspond to those of the original design point, but nevertheless within the expected data accuracy. In this table, a stage by stage comparison is conducted of the various characteristic parameters in an attempt to illustrate the existing discrepancies between experimental and calculated data and their influence on power output. Over-all experimental power output has been reduced by 47.46% with respect to the design values. The corresponding stage power reductions are 21.86% and 74.74% respectively.

Such a large reduction in power output has been introduced mostly by three factors whose influence in order of decreasing magnitude is given below.

a) Insufficient pressure drop across the turbine 26.06%.

TABLE VII

COMPARISON OF TURBINE PERFORMANCE AT THE DESIGN POINT

	Design Point	Experimental	IBM Predicted	Percent Error	Percent Error
First Stage					
Inlet Total Pressure Poo, psia	100	102.7	102.7	+2.7	0
Inlet Total Temperature Too, °F	1150	1163	1163	+1.13	0
Flow Rate W_f, lbs/min	16	14.25	14.32	10.93	.49
Stage Efficiency η_{ST}, %	57.2	46.60	48.50	18.53	4.08
Power Output HP, hp	3.408	2.663	2.693	21.86	1.13
Rotational Speed N, rpm	40,000	40,270	40,270	.67	0
Interstage & Second Stage					
Total Temperature T_{02}, °F	780	848	840	8.72	.943
Total Pressure P_{02}, psia	33.33	33.25	35.22	0	5.92
Static Pressure P_2, psia	30	27.90	29.1	7.0	4.30
Exit Static Pressure P_4, psia	6.2	18.45	19.01	197.58	3.03
Exit Total Temperature T_{04}, °F	595	747	760.8	25.55	1.85
Stage Efficiency η_{ST}, %	45.3	34.20	24.60	24.50	28.1
Power Output HP, hp	3.199	.808	.606	74.74	25
Turbine Over-All					
Isentropic Enthalpy Drop Δh_i, Btu/lb	31.630	21.72	21.20	31.33	239
Total Power Output HP_T, hp	6.607	3.471	3.299	47.46	496
Over-all Efficiency η_t, %	55.30	46.34	46.30	16.20	.86

b) Turbine over-all efficiency reduction 13.6%.

c) Turbine flow reduction 9.16%.

The magnitude of each of these factors is directly interrelated to the magnitude of the others, and they also include the influence of other secondary losses, such as increased leakage, mixing, reheat, etc.

As discussed in Section 5.2, back pressure during the various experimental runs was governed by the choked conditions prevailing at the exit of the aft scroll. Choking of this section was a combined result of slight undersizing and nonexistence of a large degree of supersaturation. Increasing of the exit scroll area would overcome choking and would allow a larger pressure drop across the turbine with a consequent predicted performance improvement of 40% over present output due to increased available energy Δh_i across the turbine and increased over-all efficiency η_t.

As illustrated in Table VII, experimental and design interstage total pressures fully agree. This agreement is explained by the fact that the 10.93% flow reduction just balances out the area deviation caused by combined effects of no supersaturation and critical pressure discrepancies.

In the same table, a comparison is conducted between the experimental data and data obtained by means of the off-design program for the same turbine input and interstage conditions. Design point predicted parameters show good agreement and correlation with the corresponding experimental data, with discrepancies within the expected accuracy shown in Section 5.2.1. Predicted output for the first stage is somewhat larger than experimental value while the opposite is true in the second stage. This latter value may be improved by assuming that the rotor shroud offers some resistance to rotor tip leakage.

5.2.3 Turbine Weight Flow

The experimentally measured flow through the turbine at various inlet conditions is presented in Figure 2. This flow was measured by adjusting the boiler feed liquid mercury pump at a certain level and observing the pressure level at the inlet to the turbine scroll. Maximum deviation from RMS curve is approximately $\pm 12\%$.

In Figure 11, the corresponding predicted flow through both the first and second stages is given for experimentally observed inlet conditions to the nozzles. Results are also tabulated in Table VIII.

TABLE VIII
PREDICTED TURBINE WEIGHT FLOW

Run	Poo psia	W_f 2nd Stage lbs/min	W_f 1st Stage lbs/min
3	122.7	16.784	17.508
6	100.2	13.755	14.022
9	93.9	13.285	13.098
14	71.7	10.031	10.23

Maximum deviation between independently calculated nozzle flows is smaller than ±1.5%. In calculating the above flows, no supersaturation was assumed in either nozzle. If some supersaturation was occurring, this assumption would only affect the second stage nozzle since the first stage stator throat conditions for most of the experimental runs were above or on the saturation line. (Assuming 4% supersatutation in the second stage nozzle and the same initial conditions gave consistently 4 - 5% more flow.) Thus, from continuity considerations between first and second stage nozzles, any substantial degree of supersaturation would seem impossible. Comparison of temperature reading with corresponding pressure saturation temperatures have indicated supersaturation of the order of .5% which is well within the experimental error.

Comparison of RMS curves of both calculated and measured flows show complete agreement with a maximum deviation of ±.3%. Such an agreement to a great extent substantiates the loss coefficients and Reynolds number correction used up to the nozzle throat in the IBM turbine off-design program.

At the design point operating conditions, the turbine measured flow has been reduced by 11%. This large deviation is attributed to the following factors:

a) Critical pressure ratio and efficiency assumed during design.

b) Fabrication discrepancies.

c) Mismatching of nozzle profile and height.

A third method was also used to establish the flow through the turbine. This method takes advantage of the interrelation that exists between total enthalpy drop across the turbine Δh_o, flow rate, W_f, and power output HP. Thus, flow was calculated from the equation:

$$W_f = \frac{33{,}000\ HP}{778.26 \Delta h_o}$$

Both power output and Δh_o were obtained from experimental data at each run. Results are tabulated in Table IX and plotted in Figure 3. Observed scatter in Figure 3 may be due to an accumulative error of both pressure and temperature on which the total enthalpy was based, and on the dynamometer reading. Additional discrepancies may have been introduced by neglecting the internal drag power consumption which should be added to the dynamometer reading. RMS curve of Figure 2 completely checks results of Figures 3 and 4.

5.3 Turbine Heat Transfer Analysis

Thermocouples embedded along the surface of the TTP housing provided temperature gradient along the axial direction as shown in Figures 12 and 13. Position of couples shown in Figure 9 was such as to divide the turbine casing into concentric ring sections perpendicular to the axis of the unit.

Probes also inserted into the flow path read the temperature state points which, along with the thermocouple readings, established temperature boundary conditions to allow an estimate of the heat losses from or to the working fluid or from the turbine casing to the surrounding. In Figure 14, inlet scroll heat losses are plotted versus turbine weight flow. Although large scatter in data exists, it is obvious that the rate of scroll heat losses increases with the rate of flow through the turbine.

Heat transfer analysis conducted for data points (1) and (3) across the turbine has yielded results as presented in Table X. Scroll losses, as indicated, seem to account for 97% of the total net turbine heat losses and means of restricting their magnitude may increase the turbine performance by as much as 2.5 efficiency points. Of the total losses indicated in Table X, .73 Btu/lb are dissipated to the package surrounded by radiation and convection while the remaining is lost through the turbine shaft, dynamometer

TABLE IX

TURBINE WEIGHT FLOW
CALCULATED FROM EXPERIMENTAL DATA

RUN NO.	hoo Btu/lb	h_{o4} Btu/lb	Δh_o Btu/lb	HP_{DYN}	$\frac{HP\ DYN}{\Delta h_o}$	$W_{f_{CALC}}$ lb/min	Poo PSIA
1	158.75	150.60	8.15	3.046	.3737	15.852	115.7
2	159.30	150.50	8.80	3.589	.4078	17.299	119.7
3	159.40	149.70	9.70	4.225	.4356	18.478	122.7
4	159.06	149.40	9.66	———	———	———	123.7
5	159.33	150.65	8.68	2.652	.3055	12.959	96.7
6	159.45	150.10	9.35	3.065	.3278	13.905	100.2
7	159.62	149.40	10.22	3.471	.3396	14.406	102.7
8	159.60	149.45	10.15	3.545	.3493	14.817	103.8
9	159.05	150.45	8.60	2.675	.3110	13.193	93.9
10	159.30	149.90	9.40	2.998	.3189	13.528	95.1
11	159.57	149.30	10.27	3.398	.3309	14.037	94.9
12	159.50	149.00	10.50	3.462	.3297	13.986	95.7
13	159.44	149.60	8.84	2.033	.2300	9.757	72.0
14	158.52	149.10	9.42	2.189	.2324	9.858	71.7
15	158.65	148.70	9.95	2.346	.2358	10.003	69.5
16	151.80	147.15	4.50	1.656	.3680	15.611	63.9
17	151.70	147.15	3.53	1.775	.5028	21.329	62.9
18	151.68	147.20	3.60	1.813	.5036	21.362	62.2

TURBINE HOUSING AXIAL SURFACE TEMPERATURE GRADIENT
RUN NOS. 9 - 12

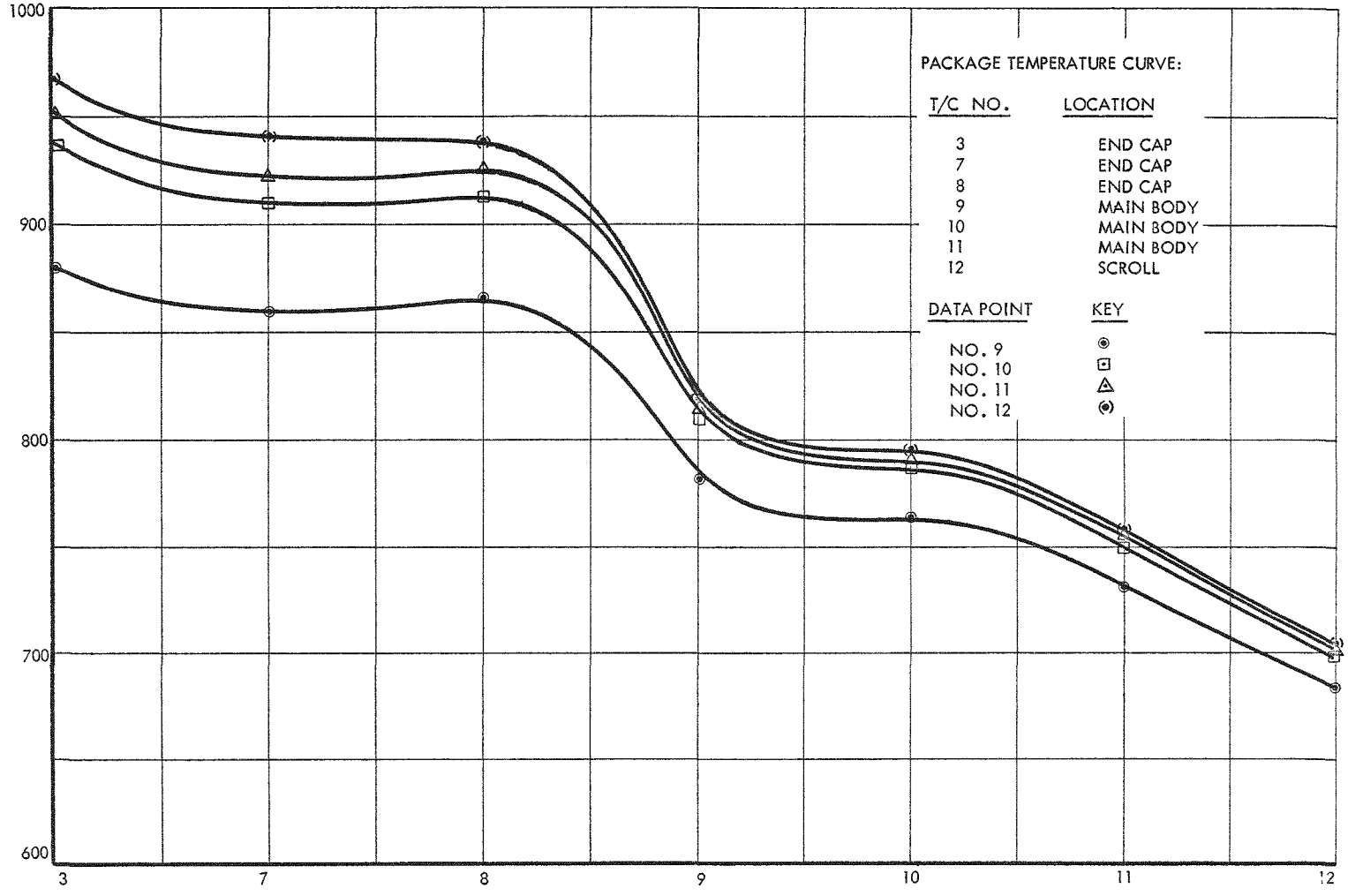

FIGURE 12

TURBINE HOUSING AXIAL SURFACE TEMPERATURE GRADIENT

RUN NOS. 16 - 18

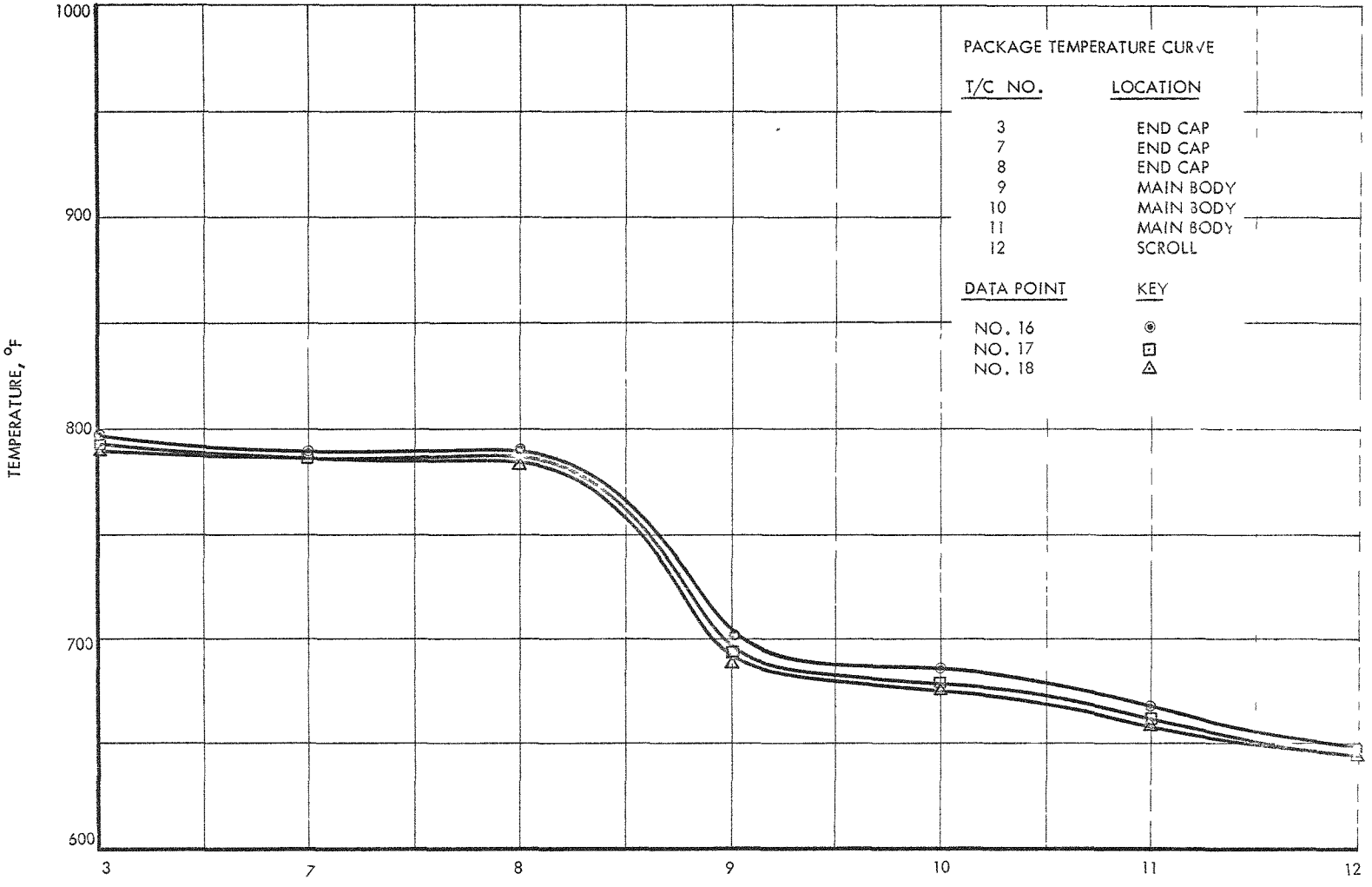

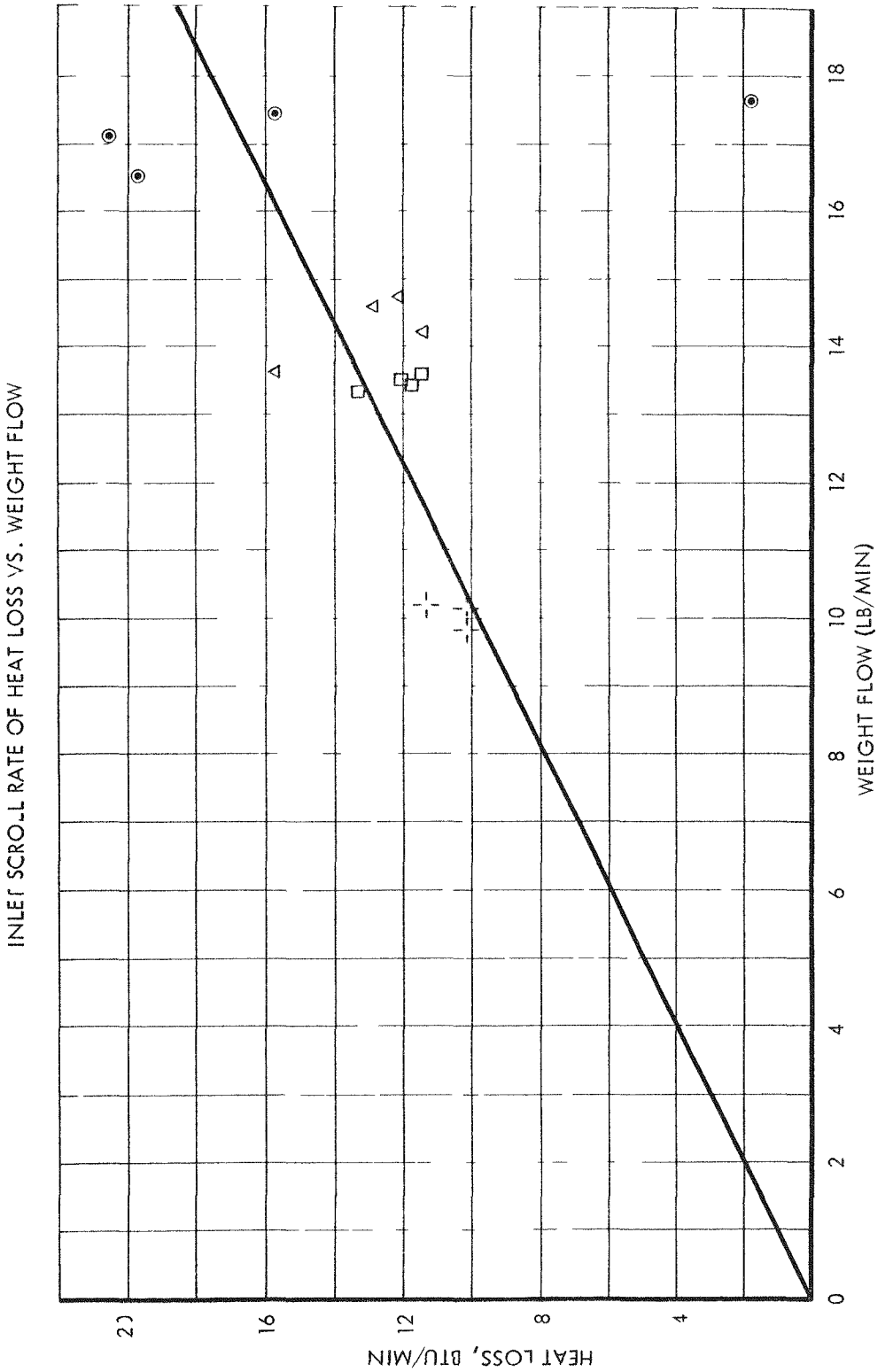
INLET SCROLL RATE OF HEAT LOSS VS. WEIGHT FLOW
HEAT LOSS, BTU/MIN
20
16
12
8
4
0
2
4
6
8
10
12
14
16
18
WEIGHT FLOW (LB/MIN)

FIGURE 14

and nitrogen high pressure seal. Of these losses, exit scroll losses are inconsequential as far as the turbine performance is concerned. Therefore, the total net heat losses would amount to 6% of total available energy across the turbine.

TABLE X
TURBINE FLOW PATH LOSSES

Zone	Data Point 1 Btu/lb	Data Point 3 Btu/lb
Inlet Scroll	-1.60	-1.33
1st Stage Nozzle	+ .20	+ .15
1st Stage Rotor	- .20	- .18
2nd Stage Nozzle	- .02	+ .06
2nd Stage Rotor	- .07	- .02
Exit Scroll	-1.17	-1.18
	-2.86	-2.50

6.0 TEST APPARATUS

6.1 Dynamometer

To obtain the highest degree of load flexibility and torque measurement accuracy, a fan absorption dynamometer with torque measurement capabilities was selected for the testing of the SNAP II Turbine.

A cross sectional view of the fan dynamometer, Figure 15, is included in this report. It can be seen, by reference to this drawing, that any developed torque output from the turbine is transmitted directly to the fan housing by fluid energy transfer, the energy eventually being dissipated as a temperature rise of the fluid. The fluid is circulated within the fan housing by passing through the fan into the diffuser then through the heat exchanger and back into the fan inlet scroll. The fan fluid temperature and the coolant temperature are monitored to keep them within safe operating limits, however, no attempt is made to measure the energy transfer to the cooling water.

Several important features of the dynamometer design are: The high speed bearing losses do not have to be considered as their torque is always included in the shaft torque measurement. Also the fan housing, which is pivoted in the trunnion bearings, provides a direct means of measuring the shaft output torque. This is accomplished by the addition of a "tee" bar to the fan housing which transmits the dynamic force to a load cell. The "tee" bar also provides a convenient and accurate means of statically calibrating the load cell.

Extreme caution was observed in the setup of the dynamometer and in the calibration of the force pickup. All of the service lines, which were connected to the fan housing, the water coolant lines to the heat exchanger, the oil mist vapor line to the high speed bearings, and the nitrogen supply line required for the pressurization of the housing, were of a soft, plastic material. The lines were heat formed into a coil to remove all stresses and carefully connected to the fan housing to minimize resisting torques. A check of the resisting torques at ambient temperature and under varying conditions of oil mist, water and nitrogen flow, indicated that a maximum (net) torque of 120 inch-grams was required to deflect the torque arm .030 inches at a lever arm of 4 inches, the movement necessary to obtain the full scale deflection of the pickup.

Because of the varying conditions induced by a changing ambient temperature, a static calibration of the load cell was performed in conjunction with each run series. The data obtained compensated for the thermal vari-

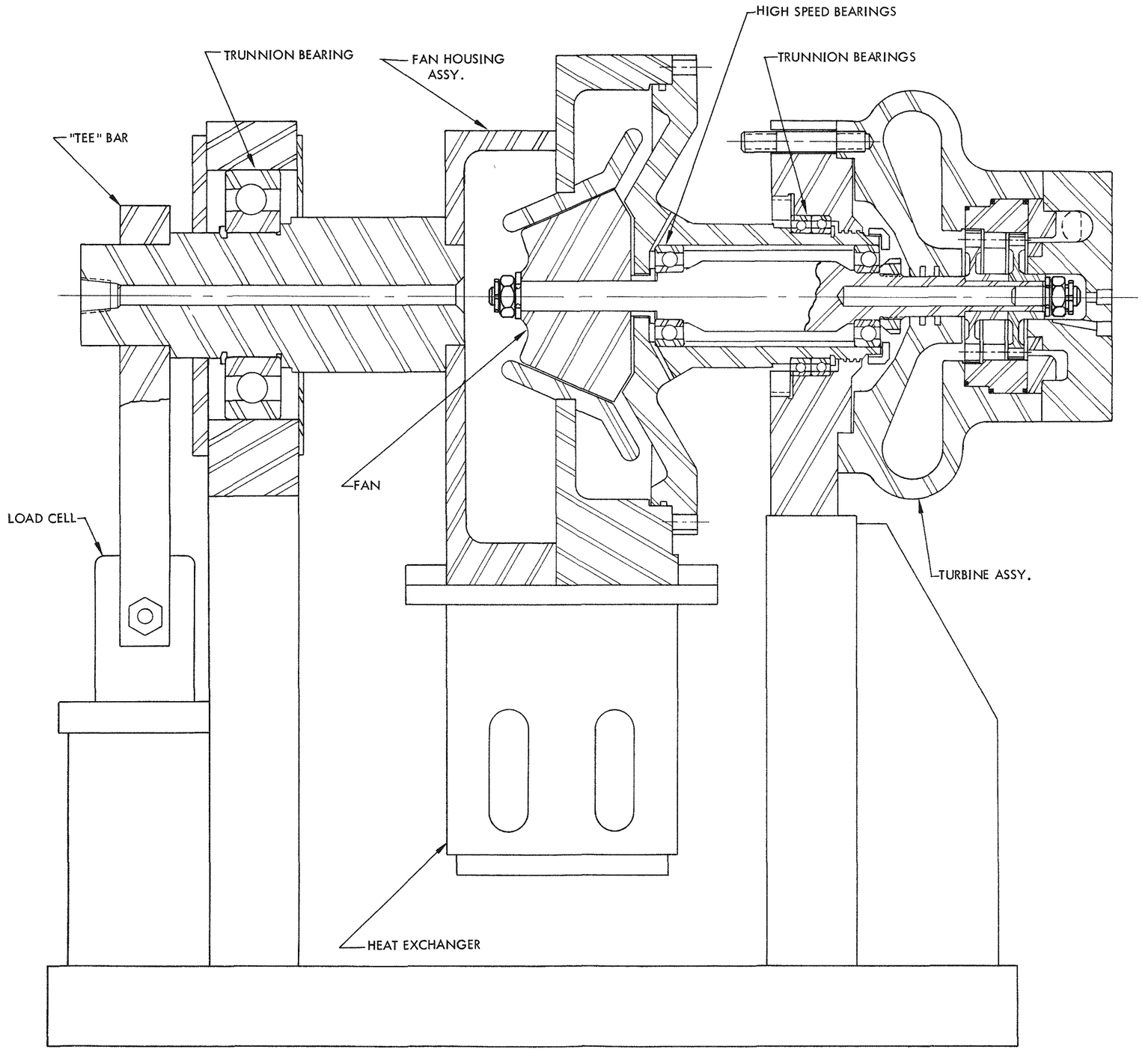

SECTIONAL VIEW OF FAN DYNAMOMETER

FIGURE 15

ations of: The spring constant in the pickup; the stiffness of the fan housing service lines; and trunnion bearing loading. No change of the fluid flows to the fan housing was made during the testing period. The calibration thus included the fluid inertia and the varying ambient temperature effects.

To preclude the possibility of losing valuable test data as a result of the load cell malfunctioning and to provide a convenient means of checking the turbine output during the hot vapor testing period, a series of fan output curves as a function of fan housing pressures was obtained. The fan output, being a function of the fan geometry and the fluid conditions, does not reflect the thermal variations in the parasitic torques of the service lines, and the high speed and trunnion bearing losses. Therefore, the power outputs, as determined from these curves, cannot be used as absolute values. They do, however, provide a rough check of the hot vapor test data and have therefore been included in this report. Figures 16 and 17 are the fan dynamometer curves which were obtained at an ambient room temperature of 75°F. Table XI illustrates the power outputs at the various test points which were obtained from the fan curves and compares them with the corresponding values of power as determined from the torque data. It can be seen that temperature effects have a marked influence on the accuracy of the fan data curves. The variations of output for each run series indicate a definite trend in the thermally induced parasitic torques.

6.2 Instrumentation

To obtain the maximum amount of information and to provide an alternate system of test data, the instrumentation which was selected for the TTP had both visual and electrical outputs where possible. The electrical signals were all photographically recorded by light beam galvanometers on a strip chart. This provided a common time base to relate the various parameters.

The following is a brief description of the various pickups and their associated equipment.

6.2.1 Temperatures

All internal thermocouple probes were chromel-alumel, completely enclosed in a .040 inch diameter stainless steel sheath, with the junction welded to the sheath to obtain a maximum rate of response. All probes were positioned perpendicular to the fluid flow and at the maximum immersion length to lessen conduction losses. The developed emf was fed to a simple voltage divider circuit which controlled the current flow to the light beam galvanometer of the recorder.

DYNAMOMETER FAN CURVES, SPEED VS. FAN LOAD

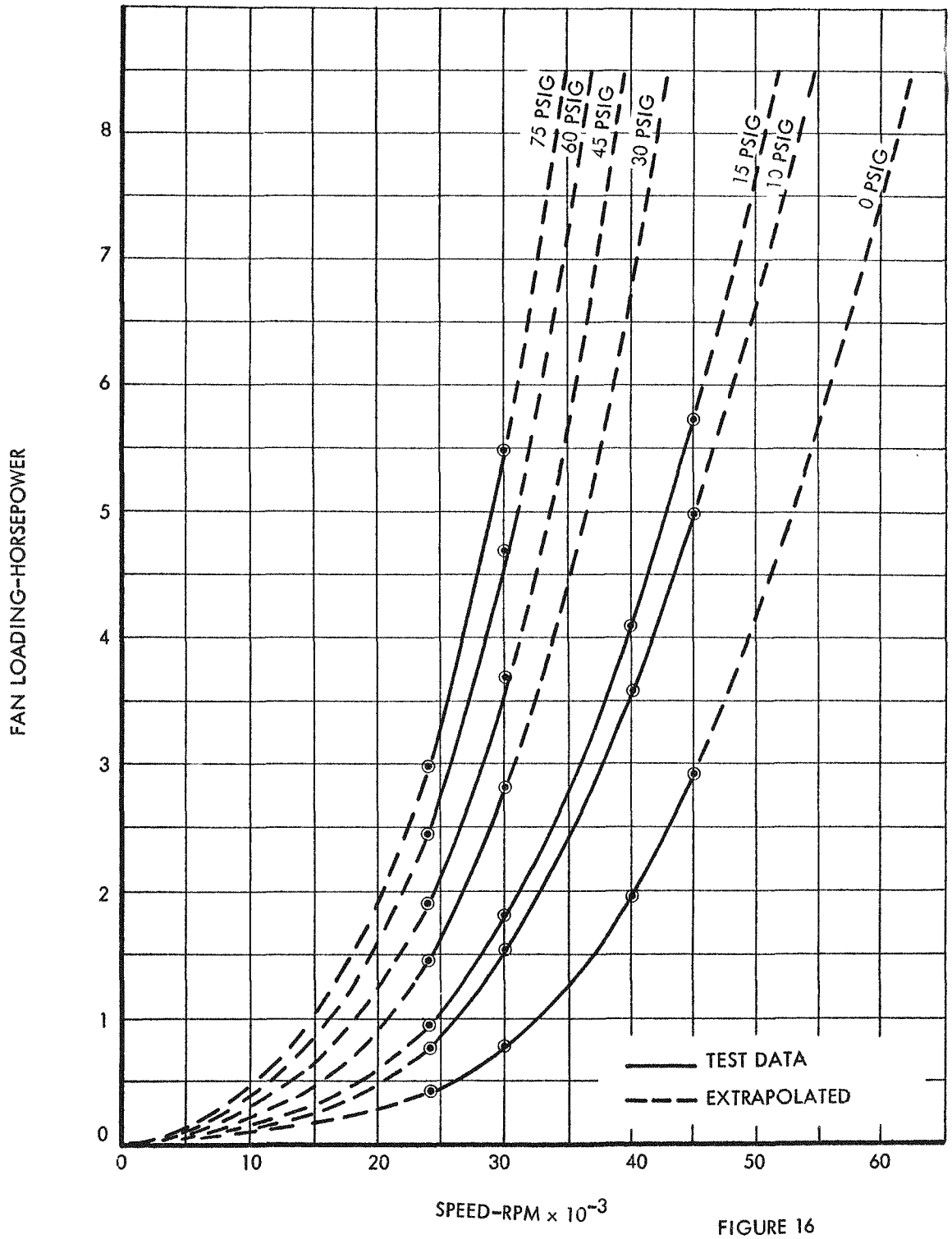

FIGURE 16

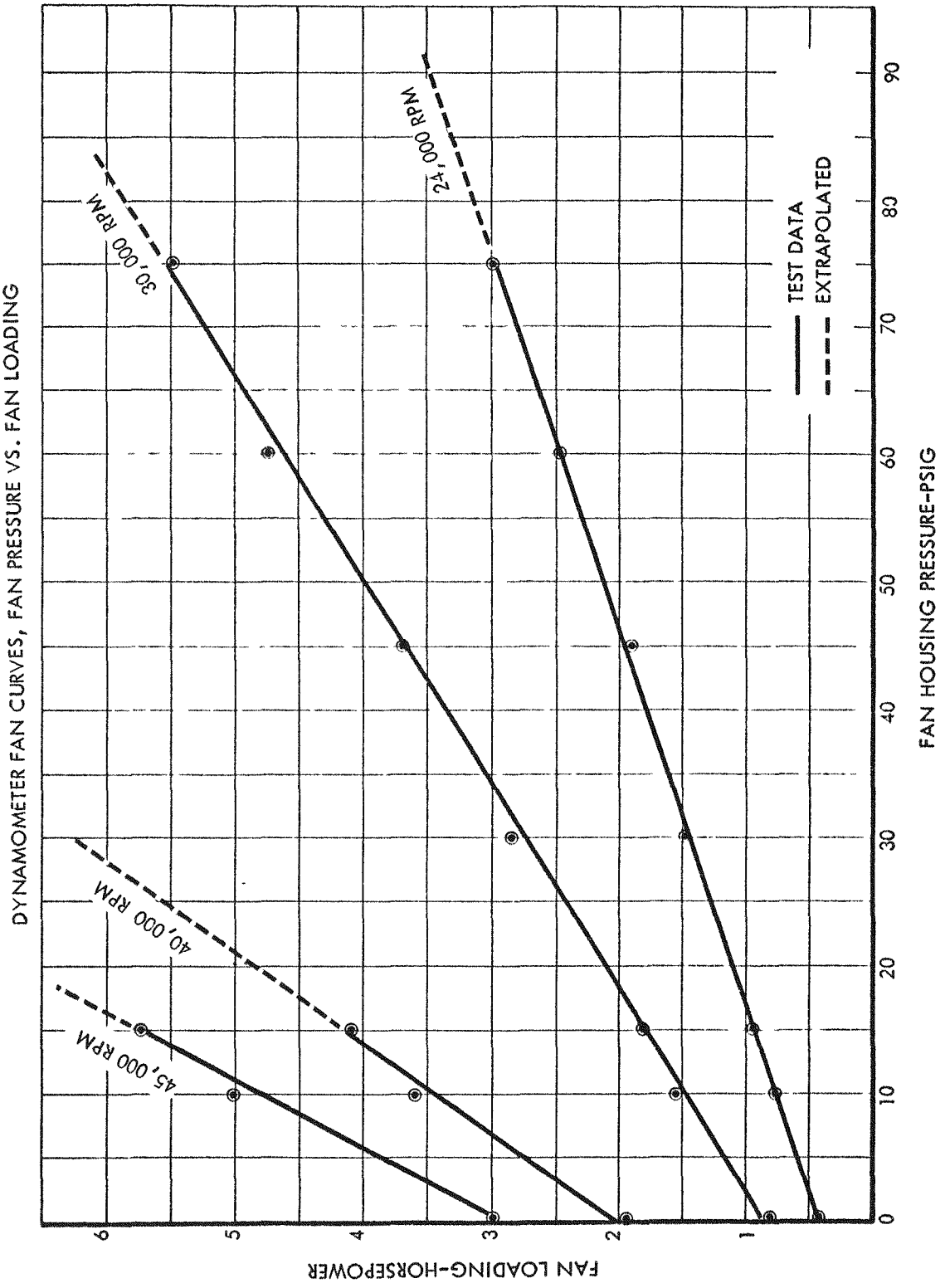
DYNAMOMETER FAN CURVES, FAN PRESSURE VS. FAN LOADING
FAN HOUSING PRESSURE-PSIG
FAN LOADING-HORSEPOWER
TEST DATA
EXTRAPOLATED
24,000 RPM
30,000 RPM
40,000 RPM
45,000 RPM
0
10
20
30
40
50
60
70
80
90
1
2
3
4
5
6

FIGURE 17

TABLE XI

DYNAMOMETER TURBINE POWER OUTPUT

Run No.	Nominal Inlet Conditions	Turbine Speed RPM	HP Torque Data	Fan Housing Pressure PSIG	HP Fan Data	Δ HP $HP_{Fan} - HP_{Torque}$	Ambient Room Temp.
1	120 psia	24,500	2.92	81.0	3.42	.5	115
2	1150°F	30,650	3.678	45.2	3.85	.172	117
3		40,800	4.060	14.9	4.37	.31	118
4		45,375		8.2	4.60		140
5	110 psia	25,600	2.655	59.2	3.08	.425	147
6	1150°F	30,500	3.065	35.8	3.20	.135	148
7		40,270	3.463	11.3	3.70	.237	149
8		45,270	3.545	4.7	3.90	.355	150
9	100 psia	24,650	2.670	65.8	2.92	.250	156
10	1150°F	30,530	2.998	33.2	3.12	.122	156
11		40,550	3.398	8.8	3.40	.002	156
12		45,800	3.458	2.5	3.55	.092	156
13	70 psia	24,700	2.033	44.9	2.18	.147	157
14	1150°F	30,750	2.197	19.8	2.25	.053	157
15		40,800	2.342	1.2	2.40	.058	157
16	70 psia	24,750	1.653	33.1	1.75	.097	156
17	T_{SAT}	30,875	1.772	11.1	1.72	-.052	156
18		35,750	1.809	2.9	1.72	-.089	156

In addition to the immersed thermocouples, a series of surface probes were pinned into milled slots in the turbine housing surface. These probes were chromel-alumel, completely enclosed in a .060 inch diameter stainless steel sheath with the junction welded to the sheath. A minimum of ten sheath diameters was pressed into the milled slot so as to lessen conduction losses from the thermocouple junction. The output from the couple was sensed by a multipoint temperature logger for intermittent recording of the surface temperatures.

6.2.2 Pressures

All of the turbine fluid pressures were sensed with bourdon tube type pressure gages which have, in addition to the dial indicator, a low torque potentiometer that is actuated from a common pinion drive. The output signal from the pickup is connected directly to the recorder galvanometer.

In the sensing of the turbine pressures, a system of pressure controls was installed which maintained an inert gas in the gage lines. The use of an inert gas in the gage lines provided a more accurate and flexible installation.

As shown in Figure 18, the Pressure Gage Inerting System operated as follows: The sensing line transmitted the turbine fluid pressure to the biasing regulator. The regulator has an adjustable pressure output which permits a flow of nitrogen at a slight increase of pressure over that which was sensed. The volume of gas flow was then controlled by dropping the pressure across a variable orifice in a Rotameter. The amount of gas volume which was permitted to enter the gage line was held to a minimum of less than 0.2 scfh. Because of the exceeding small volumes of gas introduced into the system, it was possible during transient turbine pressure rises for mercury vapor to enter the gage line and set up a condenser action. A trap was therefore provided with a slight gage to monitor the amount and the rate of condensation. No attempt was made to record turbine data until the condensing action had been stopped. The only line which showed an accumulation of condensate was the turbine inlet pressure line. This was the only pressure which experienced significant changes.

6.2.3 Turbine Speed

The turbine speed was sensed by an electromagnetic pickup which was actuated by surface variations on the high speed shaft. The

PRESSURE GAGE INERTING SYSTEM

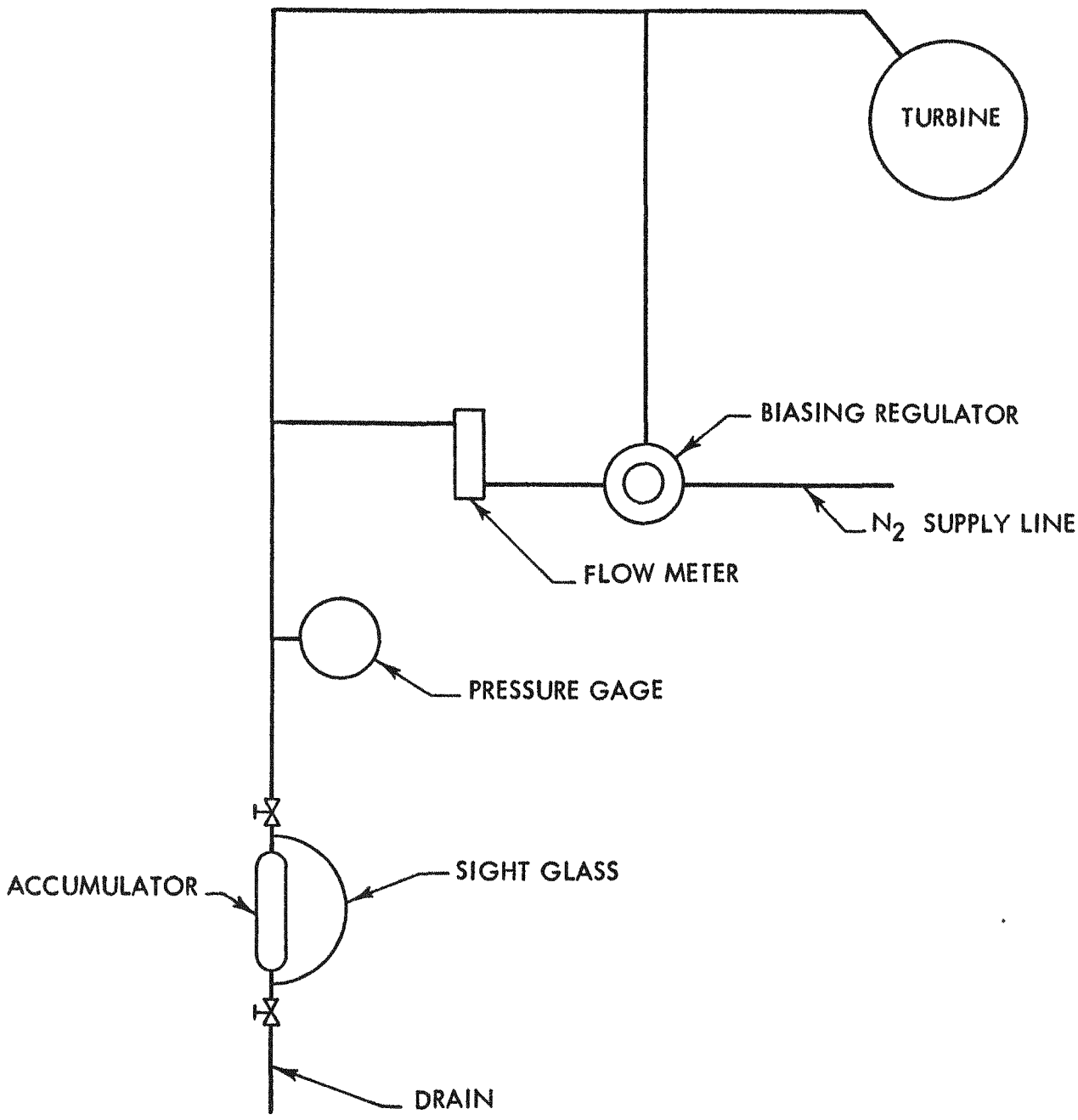

FIGURE 18

generated output signal from the pickup was directly connected to an electronic counter for visual digital readout and to a pulse converter which supplied a proportional DC signal to the recorder galvanometer.

6.2.4 Torque

The force pickup used to measure the output of the dynamometer was a linear variable differential transformer (LVDT), which has a movable core mounted on a set of cantilevered springs. The output signal of the pickup was fed into an electrical multibalance network which used another LVDT to cancel out the pickup signal. The external LVDT was directly coupled to a dial indicator for visual observation. It had been initially planned that a dynamic recording of the torque output would be made, however, because of an instrumentation malfunction and time limitations in the testing schedule, it was not possible to make the required circuit modifications. As a consequence, it was necessary to substitute a null balance, servo operated dial indicator. The null balance network, being essentially temperature stable, eliminated the electrical error and thereby made it possible to calibrate out the thermally induced errors in the cantilevered springs of the force pickup. The use of the null balance system, however, prevented the dynamic recording of the output torque. It would have been necessary to make extensive changes to the system, both electrical and mechanical to provide an output signal for the recorder.

6.2.5 Vibration

A vibration pickup was provided to monitor the high speed bearing operation.

6.3 Labyrinth Seal

One of the problems encountered in the hot vapor operation of the TTP was in the design of an effective Hg vapor seal on the high speed shaft. A compound labyrinth seal, as shown in Figure 19, Labyrinth Seal Test Schematic, was selected to minimize the possibility of mercury vapor leakage from the turbine housing and to prevent the possible infiltration of contaminants to the working fluid when the turbine pressure at that point was below room ambient conditions.

As shown in the schematic, the seal is controlled by two independent circuits. The function of the nitrogen network is to provide a positive

LABYRINTH SEAL TEST SCHEMATIC

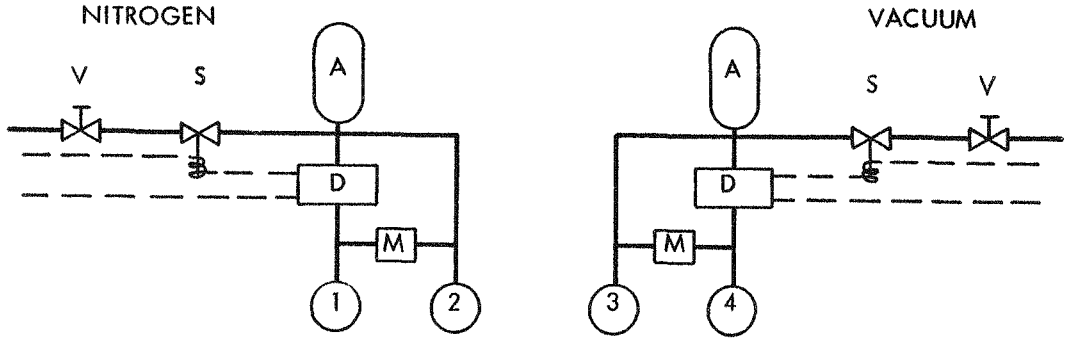

1. AMBIENT PRESSURE REFERENCE-BEARING CAVITY
2. NITROGEN SUPPLY
3. VACUUM SUPPLY
4. VACUUM REFERENCE

A. ACCUMULATOR
D. DIFFERENTIAL PRESSURE SWITCH
S. SOLENOID VALVE
V. SHUT-OFF VALVE
M. MANOMETER
PIPING
ELECTRICAL

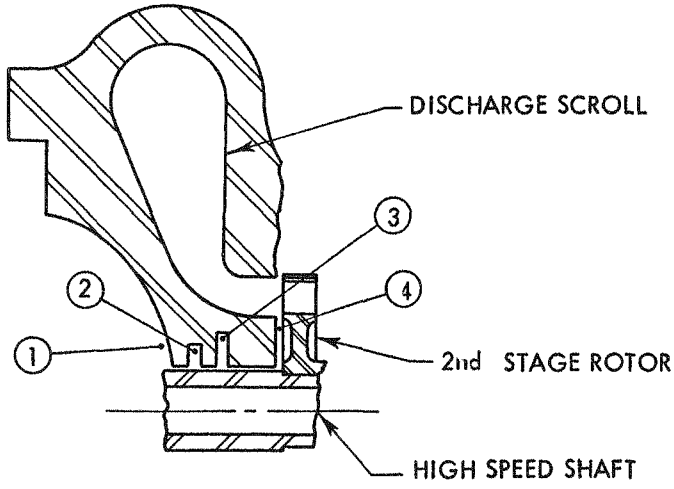

FIGURE 19

pressure at point two, in the seal, which is slightly in excess of the ambient pressure as sensed at point one. The leakage flow of the nitrogen gas to ambient inhibits the passage of contaminants through the seal. The vacuum network provides a negative pressure difference from point 4 to point 3, thereby preventing the flow of the nitrogen gas leakage into the turbine discharge scroll. In addition, the mercury vapor leakage from the turbine is drawn from the seal at this point and returned to the system.

The initital design conditions of the SNAP II turbine indicated that the system pressure at the seal would be considerably below ambient pressures. However, due to choking of the exit scroll, the system pressures at this point were mostly above ambient. As a consequence, the magnitude of the seal differential pressures was altered to correspond with the current test conditions. The required changes had little or no effect on the turbine performance.

6.4 Recommended Improvements

To present a more complete analysis of turbine performance, it is necessary in future testing that a maximum number of probes be provided in our turbine test packages. Thermocouples which were positioned in the turbine inlet scroll and in the second stage rotor discharge annulus, indicated peripheral temperature variations as large as 70°F. The combined error, which could have resulted from the omission of the multiple probes, would have been in excess of twenty percent of the total available turbine energy. It is quite possible that significant pressure gradients were also present; however, because only a single set of pressure probes per stage were provided in the TTP, no test data is available for comparison. It is recommended that at least two sets of pressure and temperature probes per stage be provided in future turbine test packages.

Some difficulty was encountered in the prevention of mercury vapor leakage at the connections to the turbine test package. In particular, on the turbine inlet line a bolted flange connection with a metallic O-ring seal consistently leaked after a short period of hot vapor operation. In contrast to this seal, a "Swagelok" union which was used on the same line showed no signs of leakage. All of the instrument line connections to the turbine housing employed metallic O-ring seals and although no leakage could be directly attributed to these seals, post hot run checks of the seals revealed various degrees of looseness. Based on general laboratory experience, it therefore appears that only welded connections are desirable for mercury vapor applications and that "Swagelok" type fittings are acceptable where requirements prohibit the use of permanent joints.

7.0 CONCLUSIONS

7.1 Turbine Design

The turbine type selected for the SNAP II Mercury Vapor System is a two-stage, axial flow, full admission turbine with some reaction across the second stage. The turbine selection was based on the following:

a. Highest predictable efficiency.

b. Compact mechanical design.

c. Compatibility with bearing load capacity.

d. Good assurance of extended life capability.

e. Reasonable, though not minimum, fabrication costs.

The SNAP II system preliminary turbine was designed, fabricated, and tested in order to determine turbine design and off-design performance.

Fabrication deviations from the design geometry dimensions have produced slight variations in turbine performance.

Nevertheless, reasonable correlation of computed and experimental performance was obtained to verify and substantiate the estimated loss coefficiencts used in conjunction with the turbine design and off-design analytical procedures.

7.2 Experimental Turbine Testing

The experimental power output of the turbine was considerably less than the design value due to the following primary reasons:

a. Insufficient pressure drop across the turbine.

b. Reduction in turbine weight flow.

The turbine weight flow at the design point was reduced by 10.93% due to the following factors:

a. Discrepancies in design assumptions and experimental results for critical pressure ratio and efficiency.

b. Fabrication discrepancies.

c. Mismatching of first stage nozzle profile and height during design.

Evaluation of the experimental turbine test results indicated the following:

a. Negligible supersaturation (less than 1%) exists throughout the Mercury Vapor Turbine. Since the turbine was initially designed assuming 4% supersaturation, the flow passages in the second stage were under size due to differences in the density and the critical pressure ratio in this nozzle.

b. Separation of the fluid from the rotor blades occurred during testing.

c. The exit scroll was choked due to a slight undersizing of the aft scroll exit and the nonexistence of a large degree of supersaturation.

d. The nozzle efficiencies and discharge coefficients as predicted by the IBM turbine programs were verified by experimental test data.

e. The critical pressure ratios obtained from perfect gas equations and used during design are quite different than the values obtained by graphical means. The critical pressure ratios as calculated by graphical means were indirectly verified by correlation of predicted and measured turbine flow.

8.0 RECOMMENDATIONS

8.1 Turbine Design

1. Neglect supersaturation in the design of small output mercury vapor turbines and modify the design and off-design computer programs accordingly.

2. Eliminate uncover turning downstream of the nozzle and rotor throats to minimize possibility of fluid separation from the guiding blade surfaces and provide improved flow direction from the nozzle and rotor and simplify the fabrication of the blading.

3. Increase the scroll exit area to increase the pressure drop across the turbine and provide an increase in the power output of the turbine.

4. Increase the mean wheel diameter in both the first and second stages in order to increase the torque arm of the rotors and attain a higher efficiency due to the increase in u/C ratio.

5. Provide labyrinth seals in the housing over the rotor shrouds to reduce leakage and increase the power output of the turbine.

6. Incorporate tapered nozzles and rotors to avoid sudden expansion losses along the flow path.

7. Calculate the critical pressure ratios in the nozzles by graphical means. This method includes the influence of such factors as internal losses, heat transfer to or from the nozzle, initial pressure and temperature, saturation or superheat phase of the vapor.

8. Minimize the heat losses from the turbine inlet and exit scrolls in order to increase the turbine over-all efficiency. This can be achieved by minimizing the heat transfer cross sectional areas and appropriate insulation of the turbine casing.

8.2 Experimental Turbine Testing

1. A maximum number of internal temperature and pressure probes should be installed in the turbine test package in order to improve the accuracy and reliability of the test data and be in a

position to investigate possible peripheral and radial temperature and pressure variations along the flow path.

2. Welded connections are recommended for sealing in mercury vapor applications. "Swagelok" type fittings are acceptable where requirements prohibit the use of permanent joints.

3. An analytical and experimental turbine erosion program should be undertaken to evaluate and reduce erosion of turbine components.

9.0 APPENDIX

9.1 Calculation Procedure for Turbine Performance Parameters

Data forms 1, 2 and 3 have been worked out to simplify and ease the calculations required for plotting the performance curves of the TDTP.

Form 1 is for the calculation of horsepower and the horsepower parameter, $\frac{HP}{Poo\sqrt{Too}}$. Columns 1, 2, 3, 6 and 7 are raw data obtained from the actual test. These data have been corrected where necessary by the Test Group. The calculation performed is based upon the HP equation:

$$HP = \frac{2\,\pi\,WDN}{33,000}$$

Since there are provisions for a counterweight to be placed at a distance of 6", the moment created must be included in the total moment, WD.

$$WD = \frac{6(CW) + 4L}{12}$$

Column 4 of the form is for the calculation of $\frac{W \times D}{5250}$ prior to multiplication by N revolutions per minute in order to give HP which is placed in column 5. 5250 is the constant used for conversion of torque and RPM to HP.

Subsequent computations are: finding the square root of Too, column 8, multiplying column 8 by column 6, Poo, to obtain Poo x $\sqrt{Too}$, and dividing HP by Poo x $\sqrt{Too}$ to obtain the $\frac{HP}{Poo\sqrt{Too}}$ parameter in column 10.

The next set of calculations, appearing in form 2, is designed to yield over-all turbine efficiency, η_t, according to the expression:

$$\eta_t = \frac{33,000\ HP}{778.26\ W_f\ \Delta h_t}$$

Columns 1, 2, 3, 4 and 9 are corrected data received from Test. Column 5 is the enthalpy obtained from a Mollier diagram for mercury from inlet conditions at the test point (Poo, Too). Column 6 is also

from the Mollier diagram, and is found by assuming isentropic enthalpy drop to the exhaust pressure, P_4. Column 7 is the difference between 5 and 6. HP, column 8, is from calculations performed in form 1. Remaining calculations consist of multiplying Δh_i by W_f, columns 7 and 9, and dividing this value into HP, then multiplying by a constant 42.4, the quotient $\frac{33,000}{778.26}$.

Column 12 contains the efficiency. Columns 13, 14, 15 and 16 are for determining u/C_t. Column 13 is obtained from the expression:

$$u = \frac{dN}{229.2}$$

Column 15 is calculated from column 14 by the expression:

$$C_t = 223.78 \sqrt{\Delta h_i}$$

The value of u/C_t, the speed parameter, is placed in column 16.

Form 3 of the calculation sheets is for the purpose of computing then parameters for the plot of $\frac{HP}{Poo\sqrt{Too}}$ versus $\frac{P4}{Poo}$. The calculations are straightforward.

Single stage performance calculations are the same as outlined here except, of course, the exhaust static pressure becomes P_2 for the first stage. For second stage calculations, the inlet conditions become P_{o2} and T_{o2}. Note that the over-all efficiency as defined here is total-to-static.

9.2 List of Symbols

Figure 9 indicates the locations of the performance test data within the SNAP turbine. Symbols used in calculations are listed and defined as follows:

C_t - theoretical spouting velocity, $\sqrt{2 \times gJ \times \Delta h_i}$, F.P.S.

CW - dynamometer counterweight, lb

D - lever arm of dynamometer, ft

d - wheel pitch diameter, in

hoo - inlet enthalpy, Btu/lb (determined from Poo and Too)

h_2 - exhaust enthalpy, single stage tests, Btu/lb

h_4 - exhaust enthalpy, over-all turbine tests, Btu/lb

Δh_i - ideal isentropic enthalpy drop, Btu/lb

L - dynamometer load, lb

N - rotational speed, RPM

Poo - inlet total pressure, psia

P_{02} - interstage total pressure, psia

P_2 - exhaust static pressure, single stage tests, psia

P_4 - exhaust static pressure, over-all turbine tests, psia

Too - inlet total temperature, ^{o}R

T_{02} - interstage total temperature, ^{o}R

u - turbine wheel pitch velocity

W - force on lever arm, lbs

W_f - flow of fluid through turbine, lb/min

η_t - efficiency, total-to-static

9.2 List of Symbols

Figure 9 indicates the locations of the performance test data within the GLASS turbine. Symbols used in calculations are listed and defined as follows:

C_t - spouting velocity, $\sqrt{2 \times gJ \times \Delta h_i}$, F.P.S.

CW - dynamometer counterweight, lb

D - lever arm of dynamometer, ft

d - wheel pitch diameter, in

hoo - inlet enthalpy, Btu/lb (determined from Poo and Too)

h_2 - exhaust enthalpy, single stage tests, Btu/lb

h_4 - exhaust enthalpy, over-all turbine tests, Btu/lb

Δh_i - ideal isentropic enthalpy drop, Btu/lb

L - dynamometer load, lb

N - rotational speed, RPM

Poo - inlet total pressure, psia

P_{02} - interstage total pressure, psia

P_2 - exhaust static pressure, single stage tests, psia

P_4 - exhaust static pressure, over-all turbine tests, psia

Too - inlet total temperature, ^oR

T_{02} - interstage total temperature, ^oR

u - turbine wheel pitch velocity

W - force on lever arm, lbs

W_f - flow of fluid through turbine, lb/min

η_t - efficiency, total-to-static

9.3 Derivation of Equations (8) and (7)

Trends observed in Figures 2 through 7 are explained analytically in this section. Although the method is not a rigorous one, it verifies the relations that exist between the turbine characteristic parameters HP, Poo, N, and u.

The method of approach is as follows:

a. Power output is related to $\Delta h_i'$, η_t, and W_f by the formula:

$$HP = a_o \eta_t W_f \Delta h_i' \qquad \text{Equation (1)}$$

b. Turbine efficiency is a function of u/c and for all practical purposes, the section to the left and below the peak as shown in Figure 4 may be considered straight.

Thus:

$$\eta_t = \frac{u}{C_t} a_3 \qquad \text{Equation (2)}$$

c. For constant inlet temperature and pressure ratio across the turbine, the isentropic enthalpy drop may be approximated from the linear relation:

$$\Delta h_i = a_5 \, Poo \qquad \text{Equation (3)}$$

d. Flow through the turbine is linearly related to inlet pressure by the simple equation:

$$W_f = a_6 \, Poo \qquad \text{Equation (4)}$$

e. For constant geometry, the tangential speed in terms of the rotational speed is given by:

$$u = a_7 N \qquad \text{Equation (5)}$$

f. By definition, spouting velocity C_t is given in terms of isentropic enthalpy drop across the turbine by the equation:

$$C_t = a_8 \sqrt{\Delta h_i} \qquad \text{Equation (6)}$$

Successive substitution of Equation (3) in Equation (6) and then Equation (6) and (5) in Equation (2), the following relation is obtained:

$$\eta_t = \frac{a_9 \times N}{\sqrt{Poo}} \qquad \text{Equation (7)}$$

Substituting Equation (7), (3) and (4) in Equation (1) yields:

$$HP = a_{10} N Poo^{1.5} \qquad \text{Equation (8)}$$

FORM 1

CALCULATION OF HP PARAMETER $\frac{HP}{Poo\ \sqrt{Too}}$

① RUN NO.	② RPM (N)	③ FORCE (L) #	④ $\frac{\text{TORQUE}^{*}}{5250 \times 10^{+9}}$	⑤ HP = (④ x N)	⑥ Poo psia	⑦ Too °R	⑧ $\sqrt{Too}$	⑨ $Poo\sqrt{Too}$	⑩ $\frac{HP \times 10^{-4}}{Poo\ \sqrt{Too}}$
1	24,500	1.880	1.192	2.920	115.7	1623	40.286	4661.1	6.265
2	30,650	1.764	1.200	3.678	119.7	1640	40.497	4847.5	7.587
3	40,800	1.569	.995	4.060	122.7	1642	40.522	4972.0	8.166
4	45,375	—	—	—	123.7	1605	40.062	4955.7	—
5	25,600	1.632	1.037	2.655	96.2	1649	40.608	3906.5	6.796
6	30,500	1.583	1.005	3.065	100.2	1642	40.522	4060.3	7.549
7	40,270	1.357	.860	3.463	102.7	1650	40.620	4171.7	8.301
8	45,270	1.233	.783	3.545	103.8	1648	40.596	4213.9	8.413
9	24,650	1.709	1.083	2.670	93.9	1630	40.373	3791.0	7.043
10	30,530	1.547	.982	2.998	95.1	1638	40.472	3848.9	7.789
11	40,550	1.320	.838	3.398	94.9	1646	40.571	3850.2	8.826
12	45,800	1.190	.755	3.458	95.7	1644	40.546	3880.3	8.912
13	24,700	1.297	.823	2.033	72.0	1608	40.100	2887.2	7.041
14	30,750	1.122	.713	2.192	71.7	1610	40.125	2877.0	7.619
15	40,800	.905	.574	2.342	69.5	1616	40,200	2793.9	8.383
16	24,750	1.053	.668	1.653	63.9	1328	36,442	2328.6	7.099
17	30,875	.905	.574	1.772	62.9	1268	35,609	2239.8	7.911
18	35,750	.798	.506	1.809	62.2	1273	35,679	2219.2	8.152

* USE PLOT OF TORQUE VS. DYNAMOMETER LOAD FOR COLUMN 4.

CW = 0 LB.

FORM 2

EFFICIENCY CALCULATION $\eta_t = \frac{33{,}000\ HP}{778\ W_f \Delta h_i}$

① RUN NO.	② P_{oo} psia	③ P_4 psia	④ T_{oo} °F	⑤ h_{oo} * Btu/lb	⑥ h_4 * Btu/lb	⑦ Δh_i Btu/lb	⑧ HP (from Form 1)	⑨ CORR. W_f lb/min	⑩ $\Delta h_i \times W_f$
1	115.7	21.45	1163	159.6	137.9	21.70	2.920	16.48	357.6
2	119.7	22.15	1180	160.3	138.2	22.10	3.678	17.04	376.6
3	122.7	22.60	1182	160.1	138.05	22.05	4.060	17.53	386.5
4	123.7	22.75	1145	159.15	137.5	21.85	-	17.87	390.5
5	96.2	17.55	1189	160.3	138.65	21.65	2.655	13.24	286.6
6	100.2	17.92	1182	160.1	138.25	21.85	3.065	13.90	303.7
7	102.7	18.45	1190	160.3	138.4	21.90	3.463	14.27	312.5
8	103.8	18.58	1188	160.23	138.4	21.83	3.545	14.47	315.8
9	93.9	16.88	1170	159.8	138.1	21.70	2.670	13.64	296.0
10	95.1	17.10	1178	160.0	138.14	21.86	2.998	13.84	3.025
11	94.9	16.48	1186	161.0	138.1	22.90	3.398	12.99	297.5
12	95.7	17.25	1184	160.15	138.35	21.80	3.458	13.19	287.5
13	72.0	13.37	1148	159.25	138.35	20.90	2.033	9.506	198.7
14	71.7	13.45	1150	159.3	138.45	20.85	2.192	9.450	197.0
15	69.5	13.37	1156	159.45	138.85	20.60	2.342	9.103	187.5
16	63.9	13.03	868	152.30	134.00	18.30	1.653	9.029	165.2
17	62.9	13.03	808	151.70	133.80	17.90	1.772	9.070	162.4
18	62.2	12.98	813	151.65	133.85	17.80	1.809	8.907	161.4

* COLUMNS 5 AND 6 ARE OBTAINED FROM MOLLIER DIAGRAM FOR MERCURY

FORM 2 (cont'd)

EFFICIENCY CALCULATION

RUN NO.	(11) $\frac{HP \times 10^{-3}}{\Delta h_i \times W_f}$	(12) $\eta_t = \frac{33{,}000 \times (11)}{778}$	(13) u * ft/sec	(14) $\eta_t \Delta h_i$	(15) C * ft/sec	(16) $\frac{u}{C}$	(17) $\sqrt{\eta_t \Delta h_i}$	(18) $\frac{\sqrt{Too}}{Poo}$	(19) $W_f \frac{\sqrt{Too}}{Poo}$
1	8.166×10^{-3}	.3464	149.7	7.517	613.6	.2440	2.742	.3482	5.738
2	9.766	.4142	187.2	9.154	677.2	.2764	3.026	.3383	5.765
3	10.500	.4454	249.2	9.821	701.3	.3553	3.134	.3303	5.790
4	—	—	277.2	—	—	—	—	.3239	5.788
5	9.264	.3929	156.4	8.506	652.8	.2396	2.917	.4221	5.589
6	10.090	.4280	186.3	9.352	684.3	.2722	3.058	.4044	5.621
7	11.080	.4700	246.0	10.293	717.9	.3427	3.208	.3952	5.640
8	11.230	.4763	276.6	10.398	721.7	.3833	3.225	.3911	5.659
9	9.020	.3826	150.6	8.302	644.7	.2335	2.881	.4111	5.607
10	9.911	.4204	186.5	9.190	678.5	.2749	3.032	.4059	5.618
11	11.422	.4845	247.7	11.095	745.4	.3323	3.331	.4293	5.577
12	12.030	.5103	279.8	11.125	746.3	.3749	3.335	.4237	5.589
13	10.230	.4339	150.9	9.069	673.8	.2240	3.011	.5569	5.294
14	11.130	.4721	187.9	9.843	702.0	.2677	3.137	.5596	5.288
15	12.490	.5298	249.2	10.914	739.4	.3370	3.304	.5784	5.265
16	10.006	.4244	151.2	7.767	623.7	.2424	2.787	.5703	5.149
17	10.910	.4628	188.6	8.284	644.0	.2929	2.878	.5661	5.135
18	11.210	.4755	218.4	8.464	651.0	.3355	2.909	.5736	5.109

* COLUMN 13, u, IS OBTAINED FROM PLOT OF u VS. RPM

COLUMN 15, c, IS OBTAINED FROM PLOT OF c VS. $\eta_t \Delta h_i$

FORM 3

PLOT OF $\frac{HP}{Poo\sqrt{Too}}$ vs. $\frac{P_4}{Poo}$ FOR VARIOUS $\frac{N}{\sqrt{Too}}$ PARAMETERS

① RUN NO.	② Poo psia	③ P_4 psia	④ Poo/P_4	⑤ N RPM	⑥ Too °R	⑦ $\sqrt{Too}$ *	⑧ $\frac{N}{\sqrt{Too}}$
1	115.7	21.45	5.394	24,500	1623	40.286	608.2
2	119.7	22.15	5.404	30,650	1640	40.497	756.8
3	122.7	22.60	5.429	40,800	1642	40.522	1006.9
4	123.7	22.75	5.437	45,375	1605	40,062	1132.6
5	96.2	17.55	5.481	25,600	1649	40,608	630.4
6	100.2	17.92	5.592	30,500	1642	40,522	752.7
7	102.7	18.45	5.566	40,270	1650	40,620	991.4
8	103.8	18.58	5.587	45,270	1648	40,596	1115.1
9	98.2	16.88	5.818	24,650	1630	40,373	610.6
10	99.7	17.10	5.830	30,530	1638	40,472	754.3
11	94.5	16.48	5.734	40,550	1646	40,571	999.5
12	95.7	17.25	5.548	45,800	1644	40,546	1129.6
13	72.0	13.37	5.385	24,700	1608	40,100	616.0
14	71.7	13.45	5.331	30,750	1610	40,125	766.4
15	69.5	13.37	5.198	40,800	1616	40,200	1014.9
16	63.9	13.03	4.904	24,750	1328	36,442	679.2
17	62.9	13.03	4.827	30,875	1268	35,609	867.1
18	62.2	12.98	4.792	35,750	1273	35,679	1002.0

* COLUMN 7 IS OBTAINED FROM COLUMN 8 FORM 1.

$\frac{HP}{Poo\sqrt{Too}}$ IS OBTAINED FROM COLUMN 10 FROM FORM 1.

DISTRIBUTION

SNAP II TOPICAL REPORTS

	No. of Copies
Air Force Ballistic Missile Division, Commander Commander, Air Force Ballistic Missile Division Hq., Air Research and Development Command, USAF P.O. Box 262 Inglewood, California For: Major George Austin	1
Air Force Special Weapons Center, Commander Commander, Air Force Special Weapons Center Technical Information & Intelligence Office Kirkland Air Force Base, New Mexico Attn: Delmer J. Trester	2
Air Technical Intelligence Center, Wright-Patterson Commander, Air Technical Intelligence Center Wright Patterson Air Force Base, Ohio Attn: H. Holzbauer, AFCIN-4B1a	3
Army Ballistic Missile Agency Commanding General, Army Ballistic Missile Agency Redstone Arsenal, Alabama Attn: ORDAB-c	4-5
Atomic Energy Commission, Washington U.S. Atomic Energy Commission Technical Reports Library Washington 25, D.C. Attn: J.M. O'Leary For: Lt. Col. G.M. Anderson, DRD Capt. John Wittry, DRD Lt. Col. Robert D. Cross, DRE R.G. Oehl, DRE Technical Reports Library	6-10
Air Research and Development Command, Commander Andrews Air Force Base Washington 25, D.C. Attn: RDTAPS, Capt. W.G. Alexander	11

	No. of Copies
*Bureau of Aeronautics Chief, Bureau of Aeronautics Washington 25, D.C. Attn: C.L. Gerhardt, NP	12
Bureau of Ordnance Chief, Bureau of Ordnance Department of the Navy Room 4110 Main Navy Building Washington 25, D.C. Attn: Maryle R. Schmidt or Laura G. Meyers (To be opened by addresses only) For: REN	13, 14, 15
Bureau of Ships, Chief Chief, Bureau of Ships Code 1500 Department of the Navy Washington 25, D.C. Attn: Melvin L. Ball	16
Chicago Operations Office (AEC) U.S. Atomic Energy Commission Chicago Operations Office P.O. Box 59 Lemont, Illinois Attn: A.I. Mulyck For: M. Klein Thomas A. Nemzek	17, 18
Chief of Naval Operations Office of the Chief of Naval Operations Department of the Navy Washington 25, D.C.	19
Conoga Park Area Office (AEC) U.S. Atomic Energy Commission Canoga Park Area Office P.O. Box 591 Canoga Park, California For: A.P. Pollman, Manager	20, 21

	No. of Copies
Department of the Army Atomic Division Office of Chief of Research and Development Department of the Army Washington 25, D.C.	22
Diamond Ordnance Fuse Laboratories Diamond Ordnance Fuse Laboratories Washington 25, D.C. Attn: ORDTL 06.33, Mrs. M.A. Hawkins	23, 24, 25
Jet Propulsion Laboratory Jet Propulsion Laboratory California Institute of Technology Pasadena 3, California Attn: I.E. Newlan, Sup., Tech. Reports Distribution	26
Lockheed Missile Systems Division Asst. AF Plant Representative Missile Systems Division Lockheed Aircraft Corporation P.O. Box 504 Sunnyvale, California	27, 28, 29, 30
Los Alamos Scientific Laboratory Los Alamos Scientific Laboratory P.O. Box 1663 Los Alamos, New Mexico	31
The Martin Company The Martin Company P.O. Box 5042, Mail No. W-711 Middle River, Maryland Attn: AEC Contract Document Custodian For: D. Rauth	32
National Aeronautics and Space Administration, Ames Ames Aeronautical Laboratory Moffett Field, California Attn: Smith J. deFrance, Director	33
National Aeronautics and Space Administration, Langley Langley Aeronautical Laboratory Langley Field, Virginia Attn: Henry J. E. Reid, Director	34

	No. of Copies
National Aeronautics and Space Administration, Lewis Lewis Flight Propulsion Laboratory 21000 Brookpark Road Cleveland 35, Ohio Attn: George Mandel	35
National Aeronautics and Space Administration, Washington National Aeronautics and Space Administration 1512 H Street, N.W. Washington 25, D.C. Attn: Dr. Addison M. Rothrock	36, 37, 38, 39, 40
Naval Ordnance Laboratory Commander, U.S. Naval Ordnance Laboratory White Oak, Silver Spring, Maryland Attn: Eve Liberman, Librarian	41, 42, 43
Naval Research Laboratory Director, Naval Research Laboratory, Code 1572 Washington 25, D.C. Attn: Mrs. Katherine H. Cass	44
Office of Naval Research Office of Naval Research Department of the Navy, Code 735 Washington 25, D.C. Attn: E.E. Sullivan For: Code 429	45
Rand Corporation Director, OSAF Project Rand Via AF Liaison Office The Rand Corporation 1 1700 Main Street Santa Monica, California Attn: F.R. Collbohm For: Dr. Huth	46
Rome Air Development Center, Commander Commander, Rome Air Development Center Griffiss Air Force Base, New York Attn: RCSG, Mr. J.L. Briggs	47

	No. of Copies
School of Aviation Medicine, Randolph AFB School of Aviation Medicine, Randolph AFB Randolph Air Force Base, Texas Attn: Col. J.E. Pickering, Department of Radiobiology	48
Thompson Ramo Wooldridge Thompson Ramo Wooldridge, Inc. Staff Research and Development New Devices P.O. Box 1610 Cleveland 4, Ohio Attn: D.L. Southam	49, 50
Union Carbide Nuclear Co. (ORNL) Union Carbide Nuclear Company X-10 Laboratory Records Department P.O. Box X Oak Ridge, Tennessee	51
University of California Radiation Laboratory, Livermore University of California Radiation Laboratory Technical Information Division P.O. Box 808 Livermore, California Attn: Clovis G. Craig For: Dr. Hayden Gordon	52
Wright Air Development Center, Commander Commander, Wright Air Development Center Wright-Patterson Air Force Base, Ohio Attn: WCACT For: G.W. Sherman, WCLEE Capt. Clarence N. Munson, WCLPS WCOS	53, 54, 55, 56
Technical Information Service Extension U.S. Atomic Energy Commission Reference Branch Technical Information Service Extension P.O. Box 62 Oak Ridge, Tennessee	57-81

	No. of Copies
AI Library Atomics International P.O. Box 309 Canoga Park, California	82-92
Thompson Ramo Wooldridge Library	93-100